nagra
National Cooperative for the
Disposal of Radioactive Waste

TECHNICAL REPORT 95-09

Some Variations of the Kristallin-I Near-Field Model

November 1995

P.A. Smith
E. Curti

Hardstrasse 73, CH-5430 Wettingen/Switzerland, Telephone +41-56-437 11 11

nagra National Cooperative for the Disposal of Radioactive Waste

TECHNICAL REPORT 95-09

Some Variations of the Kristallin-I Near-Field Model

November 1995

P.A. Smith [1)]
E. Curti [2)]

[1)] QuantiSci, Melton Mowbray, England

[2)] PSI, Würenlingen and Villigen, Switzerland

Hardstrasse 73, CH-5430 Wettingen/Switzerland, Telephone +41-56-437 11 11

This report was prepared on behalf of Nagra. The viewpoints presented and conclusions reached are those of the author(s) and do not necessarily represent those of Nagra.

Preface

The Waste Management Laboratory at the Paul Scherrer Institute is performing work to develop and test models as well as to acquire specific data relevant to performance assessments of Swiss nuclear waste repositories. These investigations are undertaken in close co-operation with, and with the partial financial support of, the National Cooperative for the Disposal of Radioactive Waste (NAGRA). The present report is issued simultaneously as a PSI-Bericht and a NAGRA Technical Report.

Vorwort

Das Labor für Entsorgung am Paul Scherrer Institut führt Arbeiten zu Sicherheitsanalysen für schweizerische nukleare Endlager durch. Sie umfassen sowohl die Entwicklung und das Testen von Modellen als auch das Gewinnen spezifischer Daten. Diese Untersuchungen werden in enger Zusammenarbeit und mit teilweiser finanzieller Unterstützung der Nationale Genossenschaft fur die Lagerung radioaktiver Abfälle (NAGRA) vorgenommen. Der vorliegende Bericht erscheint gleichzeitig als PSI-Bericht und NAGRA Technischer Bericht.

Table of Contents

Abstract

The Kristallin-I project is an integrated analysis of the final disposal of vitrified high-level radioactive waste (HLW) in the crystalline basement of Northern Switzerland. It includes an analysis of the radiological consequences of radionuclide release from a repository. This analysis employs a chain of independent models for the near-field, geosphere and biosphere. In constructing these models, processes are incorporated that are believed to be relevant to repository safety, while other processes are neglected. In the present report, a set of simplified, steady-state models of the near-field is developed to investigate the possible effects of specific processes which are neglected in the time-dependent Kristallin-I near-field model. These processes are neglected, either because (i) they are thought unlikely to occur to a significant degree, or because (ii) they are likely to make a positive contribution to the performance of the near-field barrier to radionuclide migration, but are insufficiently understood to justify incorporating them in a safety assessment. The aim of this report is to investigate whether the arguments for neglecting these processes in the Kristallin-I near-field model can be justified.

This work addresses the following topics:

– *Radionuclide transport at the bentonite-host rock interface*: the Kristallin-I near-field model allows two possible boundary conditions at the interface. Either, (i) radionuclide concentration can be set to zero (mathematically equivalent to unlimited groundwater flow), or (ii) it can be assumed that the diffusive flux out of the bentonite is equal to the advective flux into the host rock. The second boundary condition tends to the first as the flowrate increases, since, at high groundwater flowrates, the concentration at the interface tends to zero. Steady-state calculations indicate that, for the near-field parameter values adopted in Kristallin-I, at Darcy velocities above about 10^{-11} m s^{-1}, the radionuclide release to the host rock becomes flowrate-independent. However, this release is reduced by about an order of magnitude at the (smaller) Darcy velocity corresponding to the Kristallin-I Reference Case, indicating that use of the second boundary condition can substantially increase the calculated performance of the near-field.

– *Canister settlement*: in the near-field model of Kristallin-I, it is assumed that long-term settlement of canisters embedded in bentonite due to creep deformation is negligible. Although in reality only very small displacements are likely, steady-state calculations indicate that even large displacements would have little effect on the net release of radionuclides to the host rock, which would increase by less than 20 % for a canister sinking half way to the tunnel floor. This indicates that neglecting canister settlement in the calculation of radionuclide releases from the near-field is unlikely to result in significant underestimates of radiological consequences, even if the degree of settlement is far greater than expected.

– *Chemical conditions and radionuclide transport at the glass-bentonite interface*: in the near-field model of Kristallin-I it is conservatively assumed that the failed canister offers no resistance to radionuclide transport. In reality, it is likely that canister failure will be localised (in the form of a crack or a hole), and that the breached canisters will act as a barrier. A steady-state model has thus been developed to

quantify the canister resistance to radionuclide transport. It is assumed that radionuclides diffuse through a thin circumferential crack (1 μm to 1 cm in width) filled with water or with bentonite. Steady-state calculations for a bentonite-filled crack indicate that the transport resistance of the crack reduces radionuclide releases by up to an order of magnitude for a 1 cm thick crack and by more than 4 orders of magnitude for a 1 μm crack. This indicates that neglecting the transport resistance of such openings gives results which err greatly on the side of conservatism. The Kristallin-I model assumes further that reducing conditions are maintained within the bentonite, in spite of the possible formation of oxidants through water radiolysis at the waste surface. Significant diffusion of such oxidants into the bentonite would locally increase the solubility limits and decrease the sorption constants of many redox-sensitive radionuclides, resulting in higher radionuclide release rates into the host rock. However, our calculations indicate that, under realistic conditions, radiolytic oxidants would not spread significantly into the bentonite. Even with highly conservative assumptions concerning the time of canister failure and the consumption of oxidants by ferrous iron in the bentonite pore water, the redox front would penetrate less than 2 cm into the bentonite.

Zusammenfassung

Das Projekt Kristallin-I ist eine umfassende Analyse der Endlagerung verglaster hochaktiver Abfälle (HAA) im kristallinen Grundgebirge der Nordschweiz. Es schliesst unter anderem eine Analyse der radiologischen Folgen einer Nuklidfreisetzung aus dem Endlager ein. Diese Analyse stützt sich auf eine Kette unabhängiger Modelle für das Nahfeld, die Geosphäre und die Biosphäre. Bei der Entwicklung solcher Modelle wurden Prozesse berücksichtigt, die sicherheitsrelevant erscheinen, während andere Prozesse vernachlässigt wurden. Im vorliegenden Bericht werden vereinfachte stationäre Modelle des Endlagernahfeldes entwickelt, um die möglichen Auswirkungen spezifischer, im zeitabhängigen Nahfeldmodell von Kristallin-I vernachlässigter Prozesse zu untersuchen. Diese Prozesse wurden vernachlässigt, da es (i) entweder unwahrscheinlich erscheint, dass sie in bedeutendem Masse stattfinden, oder (ii) obwohl sie positiv zur Wirkung der Nahfeldbarriere beitragen, jedoch zu wenig verstanden werden, um in der Sicherheitsanalyse berücksichtigt zu werden. Dieser Bericht soll nun untersuchen, ob die Argumente, mit denen die Vernachlässigung solcher Prozesse begründet wurde, gerechtfertigt sind.

Dieser Bericht hat folgende Schwerpunkte:

- *Radionuklidtransport an der Grenzfläche Bentonit-Wirtgestein:* Das Kristallin-I Nahfeldmodell erlaubt die Wahl zwischen zwei Randbedingungen an dieser Grenzfläche. (i) Entweder kann die Radionuklidkonzentration auf Null gesetzt werden (was mathematisch einem unbegrenzten Wasserfluss entspricht), oder (ii) der diffusive Fluss aus dem Bentonit kann gleich dem advektiven Fluss ins Wirtgestein gesetzt werden. Die zweite Randbedingung liefert für grosse Flussraten die gleichen Resultate wie die erste, weil dann die Radionuklidkonzentration an der Grenzfläche gegen Null strebt. Für die in Kristallin-I verwendeten Parameterwerte und für Darcy-Geschwindigkeiten grösser als etwa 10^{-11} m s^{-1} zeigen stationäre Rechnungen, dass die Radionuklidfreisetzung unabhängig von der Flussrate wird. Setzt man hingegen die im Referenzfall von Kristallin-I verwendete (kleinere) Darcy-Geschwindigkeit ein, ist die resultierende Radionuklidfreisetzung ungefähr um eine Grössenordnung kleiner. Dies zeigt, dass Rechnungen unter Verwendung der zweiten Randbedingung eine wesentlich bessere Nahfeld-Barrierenwirkung ergeben können.

- *Absinken der Stahlbehälter im Bentonit:* Im Nahfeldmodell von Kristallin-I wird angenommen, dass das durch Kriechverformung des Bentonits verursachte langfristige Absinken der Stahlbehälter vernachlässigbar ist. Stationäre Berechnungen zeigen nun, dass selbst im Falle von grösseren Verschiebungen nur begrenzte Auswirkungen auf die Radionuklidfreisetzung zu erwarten sind. So erhält man bei einem angenommenen Absinken der Behälter um die Hälfte der maximal möglichen Distanz eine Zunahme der Freisetzung um weniger als 20%. Somit ist es unwahrscheinlich, dass die radiologischen Folgen signifikant unterschätzt werden, wenn man das Absinken der Stahlbehälter in den

Nahfeldrechnungen vernachlässigt, selbst wenn die Verschiebungen wesentlich grösser wären als erwartet.

- *Chemische Bedingungen und Radionuklidtransport an der Grenzfläche Glas-Bentonit:* Im Nahfeldmodell von Kristallin-I wird eine mögliche Barrierenwirkung undichter Behälter konservativerweise vernachlässigt. In Wirklichkeit hingegen erwartet man, dass die Behälter durch Riss- oder Lochbildung lokal undicht werden, jedoch immer noch eine Barriere für den Radionuklidtransport darstellen. Deshalb wurde ein stationäres Modell entwickelt, um die Barrierenwirkung lokal beschädigter Behälter zu quantifizieren. Dabei wurde angenommen, dass die Radionuklide durch eine schmale, 1 µm bis 1 cm breite kreisförmige Öffnung diffundieren, die mit Wasser oder mit Bentonit gefüllt ist. Stationäre Rechnungen für eine solche mit Bentonit gefüllte Öffnung zeigen, dass der dadurch gebildete Transportwiderstand die Freisetzungsraten wesentlich reduziert; und zwar bis zu einer Grössenordnung für eine 1 cm breite Öffnung und bis zu 4 Grössenordnungen für eine 1 µm breite Öffnung. Das deutet darauf hin, dass durch die Vernachlässigung des Transportwiderstandes solcher Öffnungen allzu konservative Ergebnisse berechnet werden. Ferner wird im Nahfeldmodell von Kristallin-I angenommen, dass trotz der möglichen Bildung von Oxidantien infolge von Radiolyse des Wassers an der Oberfläche der verglasten Abfälle reduzierende Bedingungen im Bentonit herrschen werden. Würden aber solche Oxidantien tief in den Bentonit eindringen, hätte dies für viele redox-sensitive Radionuklide eine lokale Zunahme der Löslichkeitslimite und eine Abnahme der Sorptionskonstante zur Folge, was zu grösseren Radionuklidfreisetzungsraten ins Wirtgestein führen würde. Unsere Rechnungen zeigen, dass unter realistischen Bedingungen solche Oxidantien kaum in den Bentonit eindringen können. Selbst bei sehr konservativen Annahmen für den Zeitpunkt des Behälterversagens und für den Abbau der Oxidantien durch Eisen(II) im Bentonitporenwasser beträgt die berechnete Eindringtiefe der Redoxfront in den Bentonit weniger als 2 cm.

Résumé

Le projet Cristallin-I est une analyse intégrale d'un dépôt final pour déchets vitrifiés de haute activité (DHA), implanté dans le socle cristallin du Nord de la Suisse. Dans le cadre de ce projet, une analyse a été effectuée afin d'évaluer les conséquences radiologiques d'un relâchement des radionucléides. Cette analyse se sert d'une chaîne de modèles indépendants pour le champ proche, la géosphère et la biosphère. En développant ces modèles on inclut les processus estimés déterminants pour la sécurité du dépôt final, tandis que d'autres sont négligés. Dans ce rapport, des modèles stationnaires simplifiés du champ proche ont été développés pour étudier les effets possibles de processus spécifiques qui ne sont pas considérés dans le modèle non-stationnaire du champ proche du projet Cristallin-I. Ces processus ont été ignorés, (i) soit parce qu'il est improbable qu'ils auront des effets significatifs, (ii) soit parce que, malgré leur probable contribution positive à la performance des barrières du champ proche, ils ne sont pas suffisamment compris pour les incorporer dans un modèle de sûreté. Le but de ce rapport est de vérifier si les arguments qui ont conduit à ignorer ces processus sont justifiés.

Ce travail comprend les sujets suivants:

- *Transport des radionucléides à l'interface bentonite-roche d'accueil*: le modèle pour le projet Cristallin-I permet de choisir entre deux conditions aux limites à cet interface. Soit (i) la concentration des radionucléides peut être choisie nulle (ce qui est mathématiquement équivalent à une vitesse d'écoulement infinie de l'eau souterraine), ou bien (ii) on peut supposer que le flux diffusif provenant de la bentonite soit égal au flux advectif dans la roche. Les deux conditions aux limites convergent lorsque la vitesse d'écoulement augmente, puisque la concentration à l'interface s'approche de zéro pour des grandes vitesses d'écoulement de l'eau souterraine. Les calculs en conditions stationnaires effectués avec les valeurs paramétriques adoptées pour Cristallin-I montrent que le relâchement de radionucléides devient indépendant de la vitesse d'écoulement dès que la vitesse de Darcy dépasse à peu près 10^{-11} m s^{-1}. Cependant, ce relâchement est réduit d'un ordre de grandeur lorsqu'on utilise la vitesse de Darcy adoptée pour le Cas de Référence de Cristallin-I, indiquant que l'utilisation de la deuxième condition limite peut augmenter sensiblement la performance du champ proche.

- *Mouvement de descente des colis*: dans le modèle du champ proche pour Cristallin-I, on suppose que le tassement par glissement des colis enveloppés dans la bentonite est négligeable même à long terme. Bien qu' en réalité on ne s'attend qu'à des déplacements minimes, les calculs stationnaires montrent que, même dans le cas de glissements importants, il y aurait un effet modeste sur le relâchement des radionucléides; celui-ci augmenterait de moins de 20% pour un déplacement d'un colis égal à la moitié de la distance jusqu'à la base du tunnel. Cela indique que la négligence du processus de glissement des colis ne devrait en toute probabilité pas conduire à des sous-estimations sensibles des conséquences radiologiques, même si les déplacements sont beaucoup plus importants que prévu.

-*Conditions chimiques et transport des radionucléides à l'interface verre-bentonite*: dans le modèle du champ proche pour Cristallin-I on suppose prudemment que les colis n'offrent aucune résistance au transport des radionucléides. Cependant il est probable que la rupture des colis soit localisée (sous la forme d'un trou ou d'une fissure), et que les colis endommagés constituent une barrière. Un modèle stationnaire a donc été développé pour quantifier la résistance des colis au transport des radionucléides. On suppose que les radionucléides diffusent par une mince fissure circulaire (avec une ouverture de 1 μm jusqu'à 1 cm) remplie d'eau ou de bentonite. Les calculs stationnaires indiquent, pour une fissure remplie de bentonite, que la résistance au transport réduit comparativement le relâchement des radionucléides jusqu'à un ordre de grandeur pour une fissure de 1 cm de large et jusqu'à plus de 4 ordres de grandeur pour une fissure de 1 μm de large. Cela indique qu'en ignorant la résistance au transport de telles fissures on obtient des résultats beaucoup trop pessimistes. De plus, le modèle pour Cristallin-I suppose que des conditions réductrices sont maintenues dans la bentonite, malgré la possible formation d'oxydants par radiolyse de l'eau à la surface des déchets. Si ces oxydants diffusent en profondeur dans la bentonite, celà causerait une augmentation de la solubilité et une diminution de la constante de sorption pour beaucoup de radionucléides sensibles au potentiel d'oxydoréduction, ce qui augmenterait le relâchement de tels radionucléides dans la roche. Nos calculs indiquent pourtant, pour des conditions réalistes, que des oxydants d'origine radiolytique ne pourraient pas pénétrer d'une façon importante dans la bentonite. Même avec des hypothèses pessimistes concernant l'instant de rupture des colis et la consommation des oxydants par les ions ferreux dans l'eau interstitielle de la bentonite, le front oxydoréducteur pénétrerait de moins de 2 cm dans la bentonite.

1. Introduction

Kristallin-I is an integrated analysis of the disposal of high-level radioactive waste in the crystalline basement of Northern Switzerland, which includes a synthesis of information from geological investigations and an exploration planning study, reported in THURY et al. (1994), and a post-closure safety assessment, reported in NAGRA (1994b). The Kristallin-I project is a milestone in the Swiss HLW disposal planning programme, formally completing the regional investigation of the crystalline basement. The conclusions of the project are summarised in NAGRA (1994a).

The HLW disposal system involves emplacement of waste in a deep repository at a depth of about 1000 m. Safety relies on multiple barriers provided by the vitrified waste-forms, engineered structures (cast steel canisters, horizontally emplaced in tunnels, that are backfilled with compacted bentonite) and a thick geological barrier (low-permeability crystalline rock). The basic features of the near-field are shown in Figure 1. The post-closure safety assessment employs a chain of models to describe radionuclide release, transport through the engineered barriers of the near-field and the natural barriers of the geosphere, dilution in near-surface aquifers, distribution in soils, sediments and water bodies, and the radiological exposure pathways to man. In constructing these models, several processes are neglected, either because they are thought unlikely to occur to a significant degree, or because they are likely to make a positive contribution to the performance of the near-field barrier, but are insufficiently understood to justify incorporating them in a safety assessment model. In a safety assessment, it is essential to demonstrate that the models used are conservative in view of all uncertainties involved. This report, which focuses on some of the processes neglected in the near-field release and transport model, aims to contribute to such a demonstration.

The governing equations of the Kristallin-I near-field model are solved by the computer code STRENG (GRINDROD et al. 1990). The model considers radionuclide release following canister failure and transport through the surrounding bentonite buffer and into the host rock immediately surrounding the emplacement tunnels. The simplifying assumptions of the model are documented in GRINDROD et al. (1990). Three of these assumptions, one concerning the treatment of the bentonite-host rock interface, one concerning the long-term behaviour of the bentonite buffer and one concerning canister failure, are selected for investigation in this report:

- *Radionuclide transport at the bentonite-host rock interface*: the Kristallin-I near-field model allows two possible boundary conditions at the interface. Either, (i) radionuclide concentration can be set to zero (equivalent to unlimited groundwater flow in the host-rock), or (ii) it can be assumed that the concentration and concentration gradient in the bentonite at the boundary are such that the diffusive flux out of the bentonite is equal to the advective flux into the host rock.

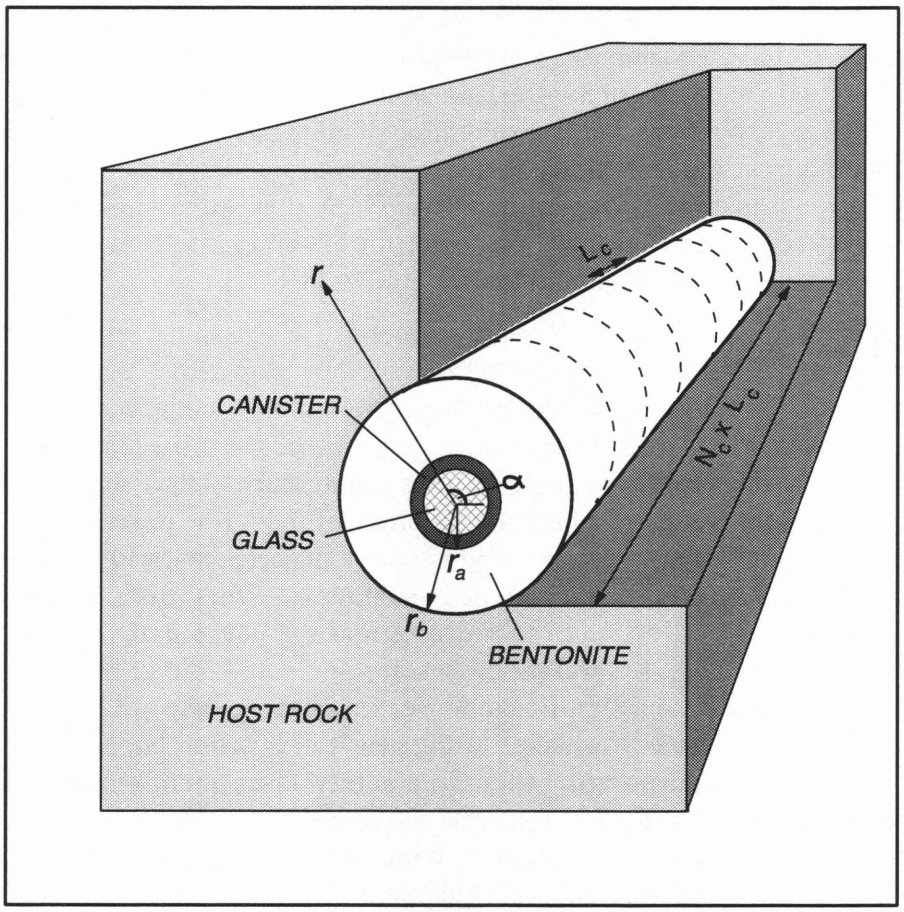

Figure 1: Model representation of the engineered barrier system considered in the Kristallin-I safety assessment, showing the cylindrical coordinate system (r,α) and some geometrical parameters used in our models. The following simplifications are made in the models: 1) the waste packages are assumed to be placed end-to-end, resulting in a single cylindrical body with length equal to the sum of all package lengths; 2) lateral diffusion from the end-faces of this body is neglected, so that cylindrical geometry results; 3) in the Kristallin-I near-field model, the physical presence of the canister is ignored following canister breaching at 1000 years after emplacement.

- *Canister settlement*: the waste packages remain centrally located within the bentonite; there are no significant errors during canister emplacement and the difference in density between the waste packages and bentonite gives no significant settlement due to creep deformation during the lifetime of the repository (~10^6 years).
- *Chemical conditions and radionuclide transport at the glass-bentonite interface*: as the canister corrodes, the metallic iron and its corrosion products provide a low oxidation potential around the waste, ensuring low solubility of many of the radionuclides. Following mechanical failure, the canisters are assumed to offer no physical resistance to radionuclide transport.

In making these simplifying assumptions, processes neglected include the following:

- *Diffusion of radionuclides from the host rock to the bentonite*: where a zero-concentration boundary condition is imposed at the bentonite-host rock interface, radionuclides passing from the bentonite are, in effect, assumed to be advected rapidly away from the near-field, without the possibility of diffusing back into the bentonite, and thus of reducing the total flux across the interface.

- *Creep deformation within the bentonite*: data from short-term compression tests on bentonite (BÖRGESSON et al. 1988), interpreted in terms of conventional soil-mechanical creep-strain equations (MITCHELL et al. 1968), indicate a rate of canister settlement that is negligible for safety assessment (WHITTLE & ARISTORENAS 1991). However, confirmation that the creep-strain equations are applicable over the very long periods required for repository safety assessment is lacking and larger canister displacements may need to be considered.

- *The effects of localised canister failure*: mechanical canister failure is, in reality, likely to be highly localised (in the form of a hole or a crack), following weakening by corrosion. Some physical resistance to radionuclide transport may therefore continue after failure, an effect which is favourable to safety. A detrimental effect, however, may arise from the release of oxidising radiolysis products from the cracks or holes, which may result in an increased oxidation potential near the waste; the resultant redox front may spread out from the point of failure through the bentonite, giving for many redox-sensitive radionuclides increased solubilities, smaller sorption constants and thus a higher rate of transport into the host rock. The release of oxidants will be more pronounced if the cracks or holes become coated with protective, non-porous layers of ferric oxides, which could form by reaction of the iron surfaces with the radiolysis products.

In order to demonstrate the conservatism of the Kristallin-I near-field model, these neglected processes must be shown either to have insignificant radiological consequences, or to make a positive contribution to the performance of the near-field as a barrier to radionuclide migration. This is achieved using a set of simplified models of the near-field, which incorporate individual processes neglected in the full safety-assessment model.

In assessing the effects on radionuclide transport of diffusion from the host rock to the bentonite, of creep deformation within the bentonite and of localised canister failure, two example radionuclides are considered:

- ^{79}Se, an example of a poorly sorbed fission product, and

- ^{237}Np, an example of a strongly sorbed nuclide[1].

The full safety-assessment near-field model considers transient diffusion and radioactive decay in the bentonite, governed, for a single nuclide with decay constant λ [y^{-1}], by the equation:

$$R_f \frac{\partial C}{\partial t} = D_p \nabla^2 C - R_f \lambda C \qquad (1)$$

where R_f [-] is a retention factor due to sorption on bentonite pores and D_p [$m^2\ y^{-1}$] is the pore diffusion coefficient, assumed to be constant in space and time. Calculations using the full safety-assessment model show, for both radionuclides, that steady-state conditions are eventually established, with a concentration in the pore water at the glass-bentonite interface equal to the elemental solubility limit[2]. For the present study, however, steady-state conditions are conservatively assumed to be established instantaneously, and to persist for a time T_L [y] until the radionuclide inventory, N_0 [mol], in the glass is exhausted. The radionuclide concentration at any point in the near-field is therefore approximated by a "top-hat" function of time. The following quantities are calculated by the simplified models:

- F_a [mol y^{-1}] and F_b [mol y^{-1}], the radionuclide release rates across the glass-bentonite interface and the bentonite-host rock interface, respectively.

- $T_L F_b / N_0$, the product of the release duration T_L [y] and the release rate to the host rock, normalised to the radionuclide initial inventory N_0.

$T_L F_b / N_0$ is a measure of the effectiveness of the near-field as a barrier to radionuclide migration. If $F_b\ T_L / N_0 = 1$, the entire inventory is released to the host rock. If $F_b\ T_L / N_0 = 0$, all the inventory decays within the near-field. T_L, the duration of release of a single nuclide from the waste glass, is given by the relation:

$$T_L = \frac{1}{\lambda} \ln\left[\frac{N_0 \lambda}{F_a} + 1\right] \qquad (2)$$

---

[1] The ingrowth of ^{237}Np from the precursors ^{245}Cm and ^{241}Am could be neglected in our simplified model, since the initial inventory of the precursors is small compared to that of ^{237}Np.

[2] In this report the beneficial effect on solubility of coprecipitating stable Se isotopes is conservatively neglected. In the Kristallin-I performance assessment this effect was taken into account, leading to a lower "effective solubility" of ^{79}Se which decreases with time due to radioactive decay.

Equation (2) is obtained through integration of the differential equation:

$$\frac{dN}{dt} = -F_a - \lambda N \tag{3}$$

by applying the boundary conditions $N(0) = N_0$ and $N(T_L) = 0$.

In modelling the effects of radiolysis on the oxidation potential within the bentonite in connection with a localised canister failure, a pessimistic production rate of radiolytic oxidants at the surface of the vitrified waste is assumed. A further assumption is that the reducing radicals produced by radiolysis are rapidly transformed into molecular hydrogen (H_2), which then behaves as an inert chemical species and does not participate to oxidation-reduction reactions. All oxidants are assumed to be transformed into molecular oxygen (O_2) on the way to the point of failure, where they start to react with the ferrous iron dissolved in the bentonite pore water. The extent to which the redox front penetrates the bentonite is calculated on the basis of a kinetic equation describing the reduction of oxygen by ferrous iron dissolved in the pore water.

The results of the model calculations presented in the following sections are given in terms of release rates integrated over the whole repository. Essentially, each model has been developed for a single canister and the results are then multiplied by the number of canisters present in the repository. This procedure implies that, in our model representation, each canister is affected by the disturbance assumed in the specific case: in the case of creep deformation within the bentonite, *all* canisters are assumed to be displaced from the centre of the tunnel by the same distance; in the case of localised canister failure, *all* canisters are supposed to be cut by a single crack, each having identical thickness and geometry.

2. Parameter Values

Parameter values used for model calculations in the present study and the corresponding mathematical symbols are given in Tables 1 (radionuclide-dependent parameters) and 2 (radionuclide-independent parameters). Additional parameter values specific to the modelling of radiolytic oxidation fronts emanating from a circumferential crack are listed in Table 6. The data in Tables 1 and 2 are those used in the Kristallin-I Reference-Case calculations.

Table 1: Radionuclide-dependent parameters for the present work.

Parameter	**Values**	
	^{79}Se	**^{237}Np**
Bentonite sorption constant, K_d [$m^3\ kg^{-1}$] *(Table 3.7.3 in NAGRA 1994b)*	0.005	5
Radionuclide half-life, ln 2 / λ [y] *(Table 3.7.1 in NAGRA 1994b)*	6.5×10^4	2.14×10^6
Inventory within the entire repository at the time of canister failure, N_0 [mol] *(Inventory per waste package given in Table 3.7.1, NAGRA 1994b; number of waste packages given in Table 2, this work)*	2.9×10^2	9.4×10^3
Solubility limit, C_S [M] * *(Table 3.7.3 in NAGRA 1994b)*	10^{-8}	10^{-10}

** Note: the solubility limit must be multiplied by a factor of 10^3 to convert from molarity [M] to mol m^{-3}, in order to substitute parameter values from this table, and from Table 2, into the equations of this report.*

Table 2: Radionuclide-independent parameters for the present work.

Parameter	**Values**
Length of fabrication container, L_C [m] (*Figure 3.4.1 in NAGRA 1994b*)	1.3
Number of waste packages, N_C [-] *(Section 3.3 in NAGRA 1994b)*	2693
Bentonite inner radius, r_a [m] (*Table 3.7.2 in NAGRA 1994b*)	0.47
Bentonite outer radius, r_b [m] (*Table 3.7.2 in NAGRA 1994b*)	1.85
Canister thickness, L [m] (*Figure 3.4.1 in NAGRA 1994b*)	0.25
Effective diffusion coefficient, $\varepsilon_p D_p$ [$m^2\ y^{-1}$] (*Table 3.7.2 in NAGRA 1994b*)	6.3×10^{-3}
Bentonite porosity, ε_p [-] (*Table 3.7.2 in NAGRA 1994b*)	0.4
Bentonite density, ρ_p [kg m^{-3}] (*Table 3.7.2 in NAGRA 1994b*)	2760

3. Radionuclide Transport at the Bentonite-Host Rock Interface

3.1 Theory

As described in Section 1, the Kristallin-I near-field model allows two possible boundary conditions at the bentonite-host rock interface. Either, (i) the radionuclide concentration can be set to zero, or (ii) it can be assumed that the concentration and concentration gradient in the bentonite at the boundary are such that the diffusive flux out of the bentonite is equal to the advective flux into the host rock. The assumption of a zero radionuclide concentration around the bentonite outer boundary is the more conservative and corresponds to the case of very high groundwater flowrates in the surrounding host rock. In this case diffusion is assumed to transport radionuclides from the bentonite to the host rock, but diffusion in the reverse direction does not occur. In this section, calculations are described which quantify the conservatism of the zero-concentration boundary condition, under the assumption of rapidly established steady-state conditions. Results obtained using boundary conditions (i) and (ii) are compared, with the aim of establishing, for a given set of near-field parameters, how large the groundwater flowrate must be in order for the two boundary conditions to yield similar solutions. This will allow the conservatism associated with boundary condition (i) to be quantified.

A cylindrical polar coordinate system (r',α) is adopted, with its origin at the centre of a waste package. The prime indicates non-dimensionalisation with respect to the length scale μ [m], where μ is given by:

$$\mu = \left(\frac{D_p}{R_f \lambda} \right)^{1/2} \qquad \text{and} \qquad r' = \frac{r}{\mu} \tag{4}$$

The retention factor, R_f [-], is given by[3]:

$$R_f = 1 + \rho_p K_d \left(\frac{1 - \varepsilon_p}{\varepsilon_p} \right) \approx \frac{\rho_p K_d}{\varepsilon_p}. \tag{5}$$

From Equation (1), in the coordinate system (r',α), steady-state radionuclide diffusion and decay in the bentonite is described by the equation:

---

[3] The approximation in Equation (5) is valid only for small values of porosity (i.e. where $\varepsilon_p << 1$). Although the errors in the retention factors of ^{79}Se and ^{237}Np introduced by using this approximation affect the results to some extent, they have no relevance for the conclusions reached, since the uncertainty of the K_d values is much larger (about one order of magnitude).

$$\frac{1}{r'^2}\frac{\partial^2 C}{\partial \alpha^2}+\frac{1}{r'}\frac{\partial}{\partial r'}\left(r'\frac{\partial C}{\partial r'}\right)-C=0, \tag{6}$$

where C [M] is the radionuclide concentration. The boundary condition at the inner boundary of the bentonite is:

$$C=C_s \qquad \text{at} \qquad r=r_a. \tag{7}$$

where C_s [M] represents the solubility limit for the element of which the radionuclide is an isotope.

The requirements (a) that the radionuclide concentration is continuous across the bentonite-host rock interface and (b) that the rate of diffusion from the bentonite to the host rock across the interface is equal to the rate at which radionuclides are transported away from the near-field by advection are expressed through the relation:

$$QC=-A\varepsilon_p D_p \frac{\partial C}{\partial r} \tag{8}$$

where:

$$A=2\pi r_b L_c N_c. \tag{9}$$

Q [$m^3\ y^{-1}$] is the groundwater flowrate through the total repository and N_c is the number of waste packages. The boundary condition at the bentonite-host rock interface is then:

$$\frac{C}{\xi}=-\frac{\partial C}{\partial r} \qquad \text{at} \quad r=r_b, \tag{10}$$

where:

$$\xi=\frac{2\pi r_b L_c N_c \varepsilon_p D_p}{Q}. \tag{11}$$

Equations (8) and (10) state that the diffusive flux of nuclide from the bentonite exactly balances the amount of nuclide transported away by advection.

Because of the symmetry of the problem, solutions of Equation (6) are sought which are functions of r' only. If $C = C(r')$, Equation (6) reduces to:

$$r'^2\frac{d^2C}{dr'^2}+r'\frac{dC}{dr'}-r'^2C=0. \tag{12}$$

Solutions of Equation (12) are the modified Bessel functions of order zero (see, for example, Ch. 9.6 in ABRAMOWITZ & STEGUN 1970). Taking a linear combination of such solutions, chosen such that the boundary condition in Equation (10) is satisfied, and denoting modified Bessel functions of ith order by $I_i(r')$ and $K_i(r')$:

$$\frac{C}{C_s} = \frac{I_0(r') + \Phi K_0(r')}{I_0(r_a') + \Phi K_0(r_a')} \tag{13}$$

where Φ is a constant, which must be fixed such that the boundary condition in Equation (10) is also satisfied. Considering that

$$\frac{dI_0(r')}{dr'} = I_1(r') \tag{14}$$

and

$$\frac{dK_0(r')}{dr'} = -K_1(r') \tag{15}$$

differentiation of Equation (13) yields:

$$\frac{1}{C_s}\frac{dC}{dr'} = \frac{I_1(r') - \Phi K_1(r')}{I_0(r_a') + \Phi K_0(r_a')}. \tag{16}$$

Substituting Equations (13) and (16) in Equation (10) and rearranging:

$$\Phi = \frac{\xi' I_1(r_b') + I_0(r_b')}{\xi' K_1(r_b') - K_0(r_b')} \tag{17}$$

where:

$$\xi' = \frac{\xi}{\mu} \tag{18}$$

The release rates across the glass-bentonite and bentonite-host rock interfaces are given, respectively, by:

$$F_a = -2\pi r_a' L_c N_c \varepsilon_p D_p C_s \left(\frac{I_1(r_a') - \Phi K_1(r_a')}{I_0(r_a') + \Phi K_0(r_a')} \right) \tag{19}$$

and

$$F_b = -2\pi r_b' L_c N_c \varepsilon_p D_p C_s \left(\frac{I_1(r_b') - \Phi K_1(r_b')}{I_0(r_a') + \Phi K_0(r_a')} \right). \tag{20}$$

At high flowrates (i.e. as $\xi \to 0$), release rates across both interfaces become independent of flowrate:

$$\left.\begin{aligned}
\Phi \rightarrow\ & -\frac{I_0(r_b')}{K_0(r_b')} \\
F_a \rightarrow\ & -2\pi\, r_a' L_c N_c \varepsilon_p D_p C_s \left(\frac{I_1(r_a')K_0(r_b') + I_0(r_b')K_1(r_a')}{I_0(r_a')K_0(r_b') - I_0(r_b')K_0(r_a')} \right) \\
F_b \rightarrow\ & -2\pi\, r_b' L_c N_c \varepsilon_p D_p C_s \left(\frac{I_1(r_b')K_0(r_b') + I_0(r_b')K_1(r_b')}{I_0(r_a')K_0(r_b') - I_0(r_b')K_0(r_a')} \right)
\end{aligned}\right\} \quad \text{as} \quad Q \rightarrow \infty . \qquad (21)$$

At low flowrates (i.e. as $\xi \rightarrow \infty$), release rates across the glass-bentonite interface again become independent of flowrate and those across the bentonite-host rock interface tend to zero:

$$\left.\begin{aligned}
\Phi \rightarrow\ & \frac{I_1(r_b')}{K_1(r_b')} \\
F_a \rightarrow\ & -2\pi\, r_a' L_c N_c \varepsilon_p D_p C_s \left(\frac{I_1(r_a')K_1(r_b') - I_1(r_b')K_1(r_a')}{I_0(r_a')K_1(r_b') + I_1(r_b')K_0(r_a')} \right) \\
F_b \rightarrow\ & 0
\end{aligned}\right\} \quad \text{as} \quad Q \rightarrow 0 . \qquad (22)$$

Noting that:

$$\left.\begin{aligned}
I_0(r') &\approx 1 \\
I_1(r') &\approx \frac{r'}{2} \\
K_0(r') &\approx -\ln(r') \\
K_1(r') &\approx \frac{1}{r'}
\end{aligned}\right\} \quad \text{for } r' << 1 \qquad (23)$$

and

$$\left.\begin{aligned}
I_0(r') &\rightarrow \infty \\
I_1(r') &\rightarrow \infty \\
K_0(r') &\rightarrow 0 \\
K_1(r') &\rightarrow 0
\end{aligned}\right\} \quad \text{as } r' \rightarrow \infty \ , \qquad (24)$$

(ABRAMOWITZ & STEGUN 1970), in the special case where $r_a' << 1$ and $r_b' >> 1$, the limiting form for the release rate across the glass-bentonite interface is the same for both high and low flowrates:

$$F_a \approx 2\pi\, r_a' L_c\, N_c\, \varepsilon_p\, D_p\, C_s \frac{K_1(r_a')}{K_0(r_a')} \approx -2\pi\, L_c\, N_c\, \varepsilon_p\, D_p\, C_s \frac{1}{\ln(r_a')} \quad . \tag{25}$$

In another special case, for high flowrates and when both r_a' and r_b' are small:

$$F_a \approx F_b \approx 2\pi\, L_c\, N_c\, \varepsilon_p\, D_p C_s \frac{1}{\ln\left(\frac{r_b'}{r_a'}\right)} . \tag{26}$$

It should be remembered that all these equations refer to steady-state conditions and therefore do not take account of transient processes. For instance, although Equation (22) predicts that release rates across the bentonite-host rock interface tend to zero as the flowrate vanishes, a transient diffusive flux would probably persist as long as radionuclides are dissolved from the waste matrix (there is likely to be interconnected host-rock porosity, in which diffusion of radionuclides can take place).

3.2 Computational Results

Table 3 and Figure 2 show the effect on the releases of the two example radionuclides ^{79}Se and ^{237}Np of accounting for a finite groundwater flowrate through the host rock. The releases across the glass-bentonite interface and the bentonite-host rock interface have been calculated, non-dimensionalised with respect to the decay constant and the initial radionuclide inventories. Also given is $F_b\, T_L / N_0$, which gives a measure of the proportion of the initial inventory N_0 which does not decay in the near-field, and is released to the host rock (see Section 1).

Irrespective of the groundwater flowrate, $F_b\, T_L / N_0 << 1$ for ^{237}Np, showing that considerable decay of this radionuclide takes place within the near-field. Values much less than unity are obtained for ^{79}Se only at low groundwater flowrates. For both example radionuclides, as expected from Equation (22), the release across the bentonite-host rock interface tends to zero at low flowrates, where groundwater flow is ineffective in advecting radionuclides away from the near-field. Also as expected from Equation (21), the release rate across the bentonite-host rock interface becomes insensitive to flowrate as this parameter is increased and the concentration at the interface tends to zero (the conservative zero-concentration boundary condition is approached).

Release across the glass-bentonite interface varies much less with flowrate, particularly in the case of ^{237}Np. In agreement with Equations (21) and (22), the release switches between two approximately constant values as the flowrate is increased (see Figure 2), with the difference between the two values much larger for ^{79}Se than for ^{237}Np (for the latter radionuclide, this difference is hardly visible in Figure 2 due to the scaling of the plot).

Table 3 : The effect of groundwater flowrate through the repository on release of ^{79}Se and ^{237}Np from a single waste package. v_d is the Darcy velocity, obtained by dividing the flowrate through the repository Q by the repository area A_{rep}. Reported are the non-dimensionalised release rates from the glass into bentonite ($F_a/\lambda N_0$) and from the bentonite to the geosphere ($F_b/\lambda N_0$). Also given is the proportion of the inventory which effectively escapes into the geosphere without decaying in the near-field ($F_b T_L/N_0$).

	^{79}Se			^{237}Np		
$v_d=Q/A_{rep}$ [m s^{-1}]	1.00×10^{-16}	1.00×10^{-12}	∞	1.00×10^{-16}	1.00×10^{-12}	∞
$\xi' = \xi / \mu$	3.66×10^{4}	3.66	0	2.02×10^{5}	2.02×10^{1}	0
$F_a/\lambda N_0$	1.63×10^{-2}	4.55×10^{-2}	0.33	2.83×10^{-3}	2.89×10^{-3}	4.02×10^{-3}
$F_b/\lambda N_0$	3.30×10^{-6}	3.03×10^{-2}	0.32	1.56×10^{-8}	1.49×10^{-4}	2.66×10^{-3}
$F_b T_L/N_0$	1.38×10^{-5}	9.50×10^{-2}	0.45	9.29×10^{-8}	8.69×10^{-4}	1.47×10^{-2}

Note: In Kristallin-I, a repository area $A_{rep} = 1.35 \times 10^5$ m^2 (2693 waste packages × 50 m^2 per waste package, see NAGRA 1994b) was assumed. These data were not available at the time when the results of this table were calculated and Project Gewähr data (NAGRA 1985), which give 126 m^2 per waste package, were assumed, yielding $A_{rep} = 3.39 \times 10^5$ m^2 (2693 × 126 m^2). The difference (a factor of about 2.5 in Q) is small with respect to other uncertainties and does not affect major conclusions.

In the case of ^{79}Se, at high flowrates the release across the glass-bentonite interface is similar to that across the bentonite-host rock interface, which is consistent with Equation (26). From the data in Tables 1 and 2, $r_a' = 0.07$ and $r_b' = 0.28$ for this radionuclide, and so Equation (26) would be expected to provide a reasonable approximation to releases. Low values of the non-dimensional bentonite inner and outer radii imply that little radioactive decay occurs within the bentonite. Substituting data from the tables into Equation (26):

$$\frac{F_a}{\lambda N_0} \approx \frac{F_b}{\lambda N_0} \approx 0.33,$$

in agreement with the exact results presented in Table 3.

In the case of ^{237}Np, the release across the glass-bentonite interface is almost independent of flowrate, which is consistent with the behaviour predicted by Equation (25). From the data in Tables 1 and 2, the non-dimensional outer radius of the bentonite does not greatly exceed unity; Equation (25) would therefore be expected to provide at best an approximate indication of releases. Substituting data from the tables into Equation (25):

$$\frac{F_a}{\lambda N_0} \approx 0.005,$$

which compares with exact results, for low and high flowrates, respectively, of 0.003 and 0.004 in Table 3. A value of $r_b' - r_a'$ which exceeds unity implies that significant radioactive decay occurs within the bentonite. The ^{237}Np concentration profile in the bentonite is determined primarily by decay during diffusion and by the very low solubility limit.

In spite of the fact that the half-life of ^{79}Se is 30 times smaller than that of ^{237}Np, the latter nuclide decays more effectively within the near-field due to its much higher sorption constant (by 3 orders of magnitude, see Table 1). The effect of decay results in a very small concentration, and concentration gradient, at the bentonite-host rock interface compared to those at the glass-bentonite interface, even at very high flowrates. Therefore the flux of ^{237}Np across the glass-bentonite interface is relatively unaffected by conditions imposed at the outer boundary by the groundwater flowrate. In the case of ^{79}Se, decay during diffusion is less, and the solubility limit higher (by 2 orders of magnitude, see Table 1). At high groundwater flowrates, the concentration profile is determined by the flowrate, rather than by decay, and the flux across the glass-bentonite interface will thus be sensitive to this parameter.

In Kristallin-I, the flowrate through the repository host rock (the low-permeability domain of the crystalline basement of Northern Switzerland in Reference Area West), expressed as a Darcy velocity, is, on the basis of hydrogeological modelling (THURY et al. 1994), thought to lie in the range 2×10^{-6} m y^{-1} (5×10^{-14} m s^{-1}) to 1×10^{-3} m y^{-1} (3×10^{-11} m s^{-1}). In the Reference Case, a Darcy velocity of 2×10^{-5} m y^{-1} (5×10^{-13} m s^{-1}) is assumed; see Table 3.7.6a in NAGRA (1994b). Referring to Figure 2, the release of both example radionuclides to the host rock, but particularly that of ^{237}Np, is therefore sensitive to the magnitude of the groundwater flowrate. The zero-concentration boundary condition, corresponding to groundwater flowrates larger than about 10^{-11} m s^{-1}, is shown in Figure 2 to be a conservative approximation, giving releases that are higher by about an order of magnitude than those calculated when the finite groundwater flow is taken into account.

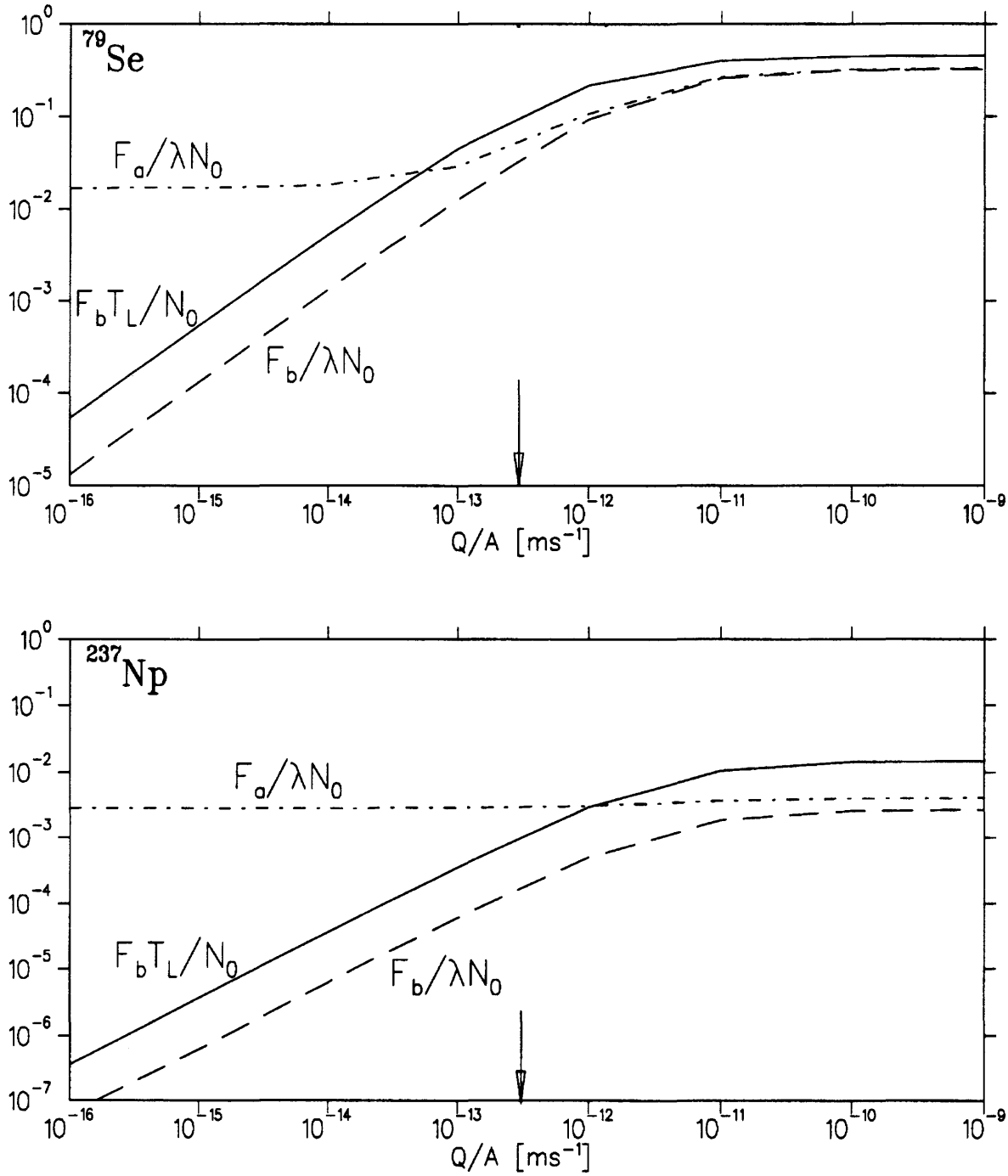

Figure 2: The effect of groundwater flowrate on the release of ^{79}Se and ^{237}Np from a single waste package. Non-dimensionalised release rates across the glass-bentonite interface (F_a / λN_0) and the bentonite-host rock interface (F_b / λN_0) are shown. $F_b T_L$ / N_0 gives an indication of the proportion of the initial inventory N_0 released to the host rock. The flowrate is expressed as a Darcy velocity, the flowrate per unit area. Arrows indicate the Darcy velocity used in the Kristallin-I Reference Case.

4. Canister Sinking

4.1 Theory

A key assumption of the Kristallin-I safety assessment is that the waste package remains surrounded by a layer of compacted bentonite over the time scales of concern (~ 10^6 years), thus retarding solute transport and preventing the movement of colloids. If the canisters were able to sink through the bentonite under gravity, then the effectiveness of the bentonite barrier could be lost. Results of calculations of canister settlement, based on conventional soil-mechanical creep-strain equations, indicate a maximum sinking of 1 to 5 mm in 10 000 years, with a rate of sinking that decreases with time (WHITTLE & ARISTORENAS 1991).

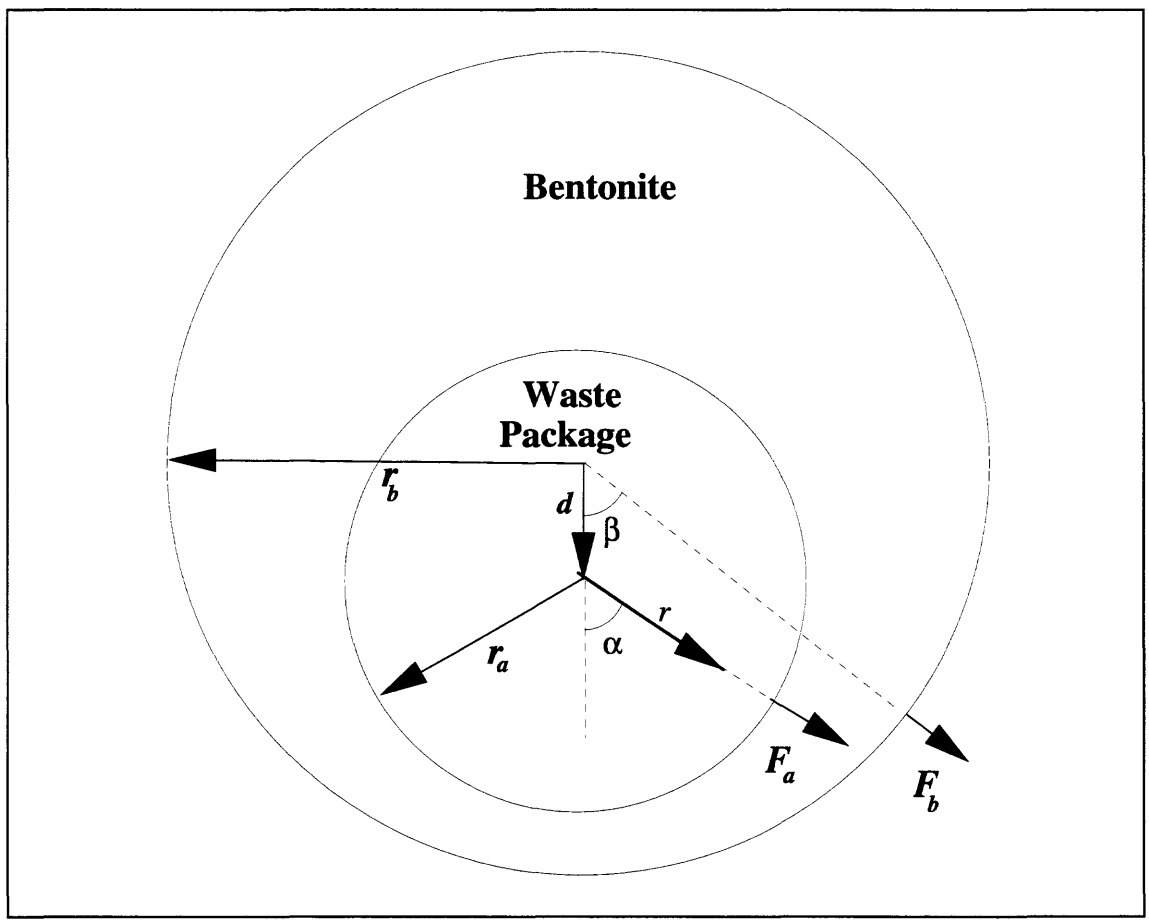

Figure 3: A waste package with its axis displaced a distance *d* from the centre of the surrounding bentonite annulus.

This amount of canister displacement is negligible for safety assessment. However, uncertainties in the selected creep properties can increase these settlements by up to an order of magnitude and confirmation that the creep-strain equations are applicable over the very long periods required for repository safety assessment is lacking. In this section, the effect on radionuclide release from the near-field following a displacement of the central axis of the waste package is examined.

The geometrical parameters describing the problem are illustrated in Figure 3. As before, a cylindrical polar coordinate system (r',α) is adopted, with its origin at the centre of the waste package (but displaced a distance d from the centre of the surrounding bentonite annulus).

The radionuclide fluxes across the glass-bentonite interface, $f_a(\alpha)$ [mol m^{-2} y^{-1}], and across the bentonite-host rock interface, $f_b(\beta)$ [mol m^{-2} y^{-1}], are obtained from a solution $C(\alpha,r')$ to Equation (6), appropriate to the geometry shown in Figure 3. Along the glass-bentonite interface (i.e. along the curve $r = r_a$),

$$f_a(\alpha) = -\varepsilon_p D_p \frac{1}{\mu}\frac{\partial C}{\partial r'} \tag{27}$$

and, along the bentonite-host rock interface ($r = \sqrt{r_b^2 - d^2 \sin^2\alpha} \quad - d\cos\alpha$),

$$f_b(\beta) = -\varepsilon_p D_p \frac{1}{\mu}\left[\cos(\alpha-\beta)\frac{\partial C}{\partial r'} - \frac{\sin(\alpha-\beta)}{r'}\frac{\partial C}{\partial \alpha}\right], \tag{28}$$

The solution $C(\alpha,r')$ is derived in Appendix I and is given by Equation (I.14). F_a and F_b, the release rates from the crack to the bentonite and from the bentonite to the host rock for the whole repository, are obtained by numerical integration of f_a and f_b along the interfaces and multiplication of the result by the length of one package and by the number of canisters in the repository, N_c:

$$F_a = r_a L_c N_c \int_{\alpha=0}^{2\pi} f_a d\alpha \tag{29}$$

and

$$F_b = r_b L_c N_c \int_{\beta=0}^{2\pi} f_b d\beta \,. \tag{30}$$

4.2 Computational Results

Table 4 and Figure 4 show the effects of canister displacement (settlement) on the releases of the two example radionuclides ^{79}Se and ^{237}Np. Canister displacement is quantified as a percentage of the maximum possible (i.e. a canister resting on the floor of the tunnel, with $d = r_b - r_a$, would have a 100% displacement). Displacements of up to 50% were calculated. Calculations for larger displacements were found to be impossible with the procedure described in Appendix I.

Even at a displacement of 50%, $F_b T_L / N_0 << 1$ for ^{237}Np, showing that almost all of this radionuclide continues to decay within the near-field. Although the value of $F_b T_L / N_0$ is higher for ^{79}Se, sensitivity of the integrated fluxes across both interfaces to displacement is also very low. At 50% displacement the integrated fluxes across the bentonite inner boundary are increased by about 15% and 9% for ^{79}Se and ^{237}Np, respectively, while those from the bentonite to the host rock are increased by about 12% and 20%, respectively. Such changes are negligible compared to the parameter uncertainties.

Table 4: Release of ^{79}Se and ^{237}Np from a displaced canister. Canister displacement is measured relative to the maximum possible displacement. T_L: duration of release from canister, F_a: release rate across the glass-bentonite interface, F_b: release rate across the bentonite-host rock interface, $f_b(\pi) / f_b(0)$: ratio of minimum flux to maximum flux from the bentonite to the host rock, N_0: initial radionuclide inventory, λ: radioactive decay constant.

	^{79}Se		^{237}Np	
Canister Displacement [%]	0	50	0	50
$F_a / \lambda N_0$	0.33	0.38	4.02×10^{-3}	4.39×10^{-3}
$F_b / \lambda N_0$	0.33	0.37	2.66×10^{-3}	3.18×10^{-3}
$F_b T_L / N_0$	0.45	0.48	1.47×10^{-2}	1.73×10^{-2}
$f_b(\pi) / f_b(0)$	1	0.17	1	0.11

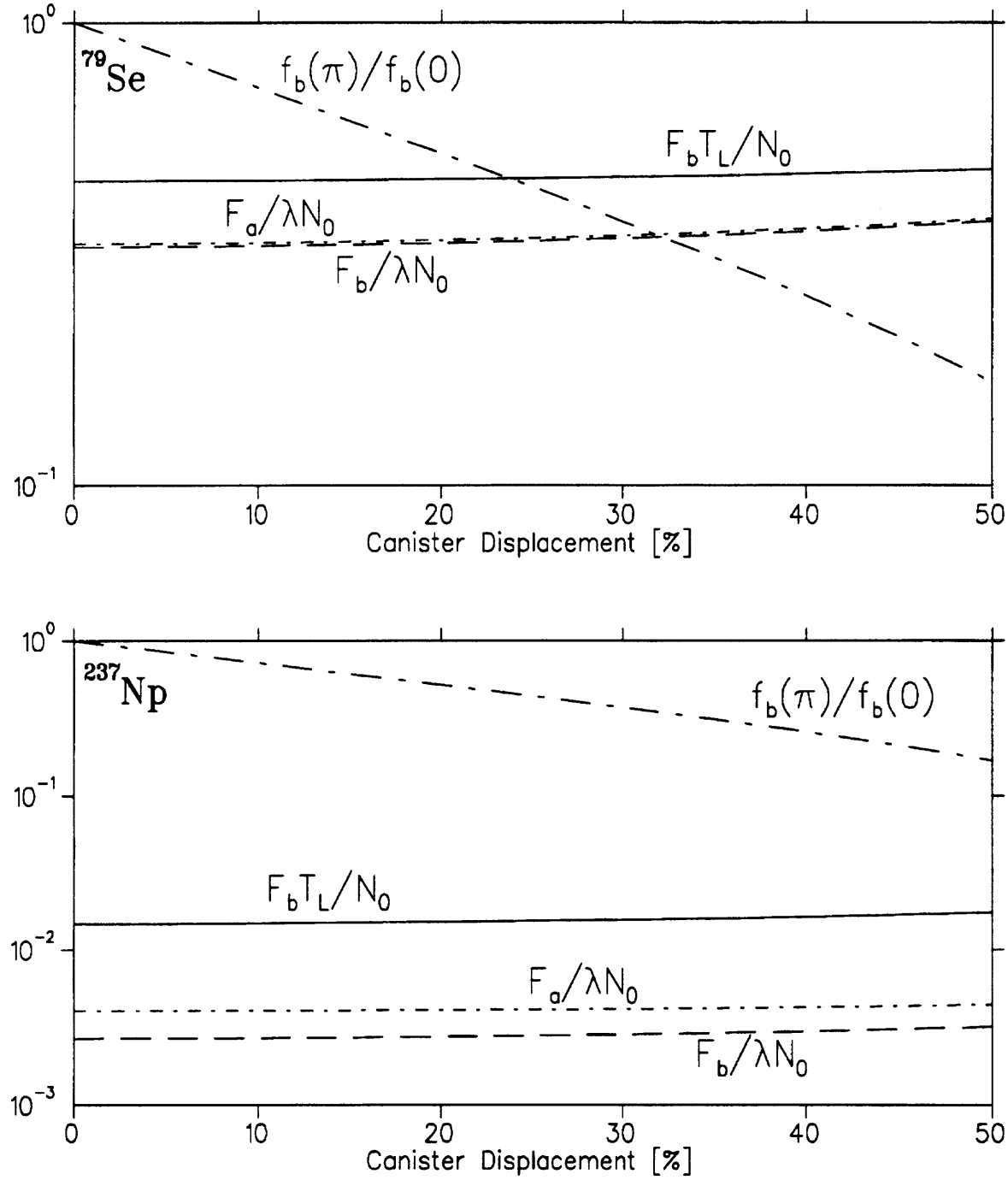

Figure 4: The effect of canister displacement (settlement) on the release of ^{79}Se and ^{237}Np from a single waste package. Non-dimensionalised release rates across the glass-bentonite interface (F_a / λN_0) and across the bentonite-host rock interface (F_b / λN_0) are shown. $F_b\ T_L$ / N_0 gives an indication of the proportion of the initial inventory released from the near-field to the host rock. The radionuclide fluxes (release rate per unit area) across the bentonite-host rock interface, calculated at $\alpha = 0$ and $\alpha = \pi$ and expressed as the ratio ($f_b(\pi)$ / $f_b(0)$), are also shown.

The radionuclide flux around the bentonite-host rock interface, however, becomes quite non-uniform as the canister is displaced. In Table 4 and Figure 4, the ratio of minimum to maximum flux across the interface, $f_b(\pi) / f_b(0)$, is given as a function of displacement. The minimum and maximum fluxes differ by factors of about 6 and 9 at 50% displacement for ^{79}Se and ^{237}Np, respectively.

5. Radionuclide and Radiolytic Oxidant Transport at the Glass-Bentonite Interface

The Kristallin-I near-field model conservatively assumes that, after failure, the canister offers no resistance to radionuclide transport. In reality, mechanical failure of the canister is likely to be localised and, for long periods of time thereafter, the resultant crack or hole may be the sole route for nuclide transport from the corroding glass to the inner surface of the bentonite. In addition to the beneficial physical effects of this transport resistance, there is also a possible detrimental chemical effect arising from the release of radiolytic oxidants, which could lead to a loss of reducing conditions in the bentonite pore water, and consequently to higher solubilities and reduced sorption for certain redox-sensitive radionuclides. The release of oxidants to the bentonite would be facilitated if a non-porous coating of ferric iron oxides (for example hematite or goethite) would form on the surfaces of the hole or crack soon after canister failure. Calculations in this section address both physical and chemical effects.

5.1 Diffusion of Radionuclides through a Cracked Canister

5.1.1 Theory

In the calculations, it is assumed that the waste package is intersected by a thin (up to about 1 cm in width), circumferential fracture lying normal to its symmetry axis. Transport calculations through perforations in a hypothetical canister of zero-thickness have also been reported in CHAMBRÉ et al. (1987). Errors in the conclusions from these calculations were discussed by AIDUN et al. (1988), who showed the importance of considering the finite wall-thickness of the canister in which the perforation occurs. The calculations performed in the present work are new in that they consider diffusion through a finite layer of bentonite surrounding the failed canister, rather than direct release to the host-rock.

Three sets of calculations have been carried out to quantify the transport resistance provided by the failed canister, coupled with that of the surrounding bentonite. The calculations are described in order of increasing realism (reducing conservatism). The first considers only the transport resistance of an annular bentonite region (effectively, zero canister thickness), although the limited size of the radionuclide source (the dimensions of the crack on the outer surface of the canister) is taken into account. This set of calculations is performed to provide comparison with calculations in which a finite canister thickness is assumed, thus showing the effects of the resistance provided by the crack. In the second set of calculations, the resistance provided by a water-filled crack is considered. Finally, as is most likely, the crack is assumed to be filled with bentonite (and/or porous canister corrosion products).

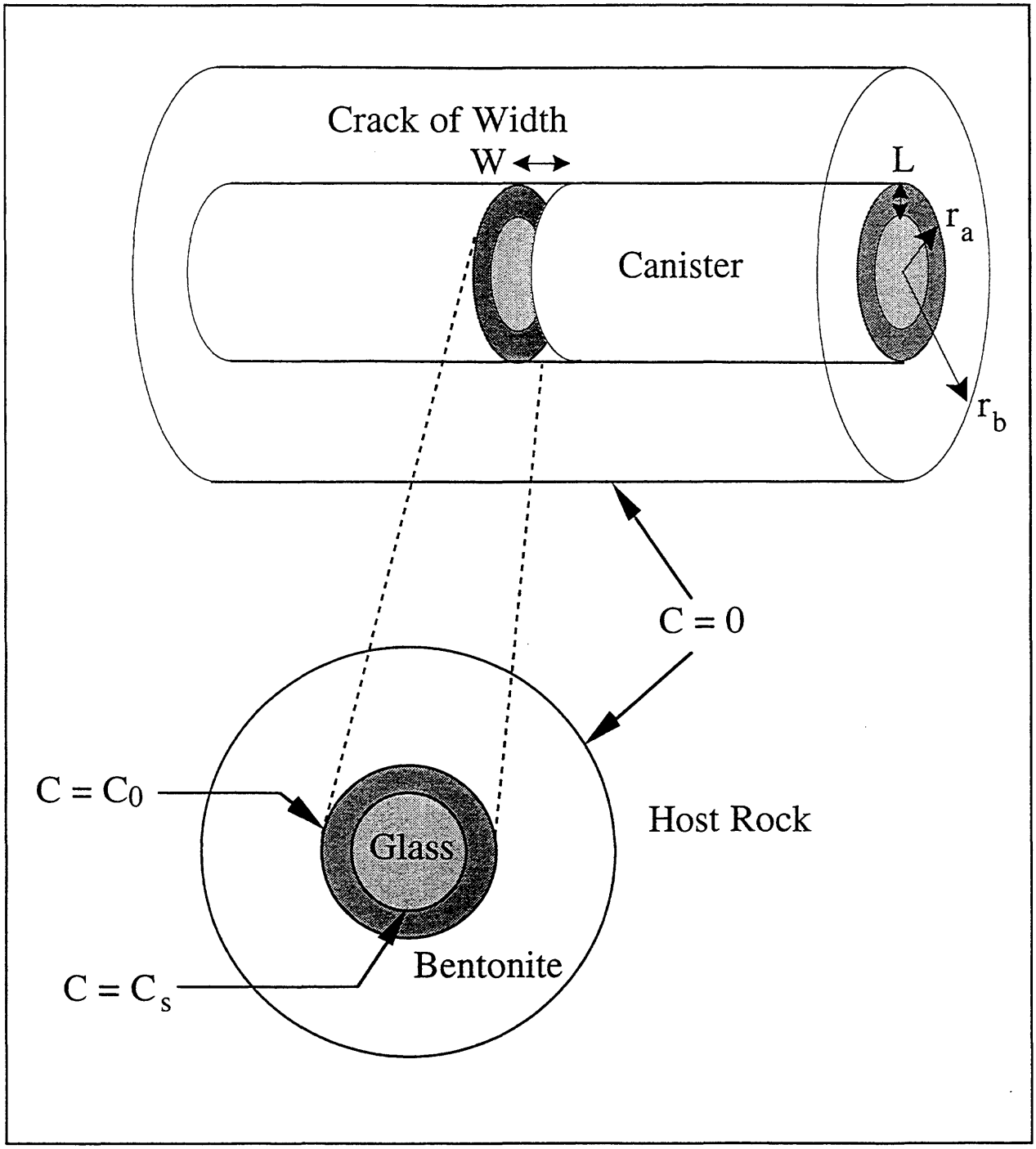

Figure 5: Geometrical parameters and boundary conditions for a cracked canister. Concentration is fixed at the solubility limit C_s at the inner surface of the canister and at zero at the bentonite-host rock interface. C_0 is the radionuclide concentration at the interface between the crack and the annular region of bentonite surrounding the canister; this is determined by solving the governing equations for diffusion both in the crack and in the surrounding bentonite.

We do not consider the case of a crack filled with hydrogen gas produced by the anaerobic corrosion of steel, because it strongly reduces conservatism in our model. In the absence of an aqueous phase, glass corrosion (and consequently radionuclide release) is expected to cease. Transport of volatile radionuclides in the gas phase can also be ruled out, as these are absent in the waste inventory. Radionuclides could possibly be transported as suspended particles if the gas bubbles out. This scenario, however, deviates considerably from that outlined by our model, since the escaping gas could threaten the integrity of the bentonite backfill and a simple diffusive model could no longer be applied. For a discussion of the problems related to gas formation in the repository, the reader is referred to NAGRA (1994b) and references therein.

The geometrical parameters describing the problem and the model used to address it are shown in Figure 5. The crack is of width W [m] and penetrates a canister of thickness L [m]. In reality, the thickness of the canister (0.25 m) is likely to be reduced by corrosion before mechanical failure occurs; the canister design includes a corrosion allowance of 5 cm (NAGRA 1994b) which is neglected in the present analysis.

The following additional assumptions are made in modelling its transport resistance:

- the crack is narrow compared to the dimensions of the surrounding bentonite annulus; the crack is thus treated as a line-source when calculating diffusion through the bentonite;
- the curvature of the annular regions occupied by the bentonite and the canister is neglected; i.e. both the canister and the bentonite are treated as rectangular blocks.
- transport within the waste package itself is assumed instantaneous, i.e. possible transport resistance within the fractured glass is neglected, so that the concentration at the inner surface of the canister is always maintained at the solubility limit C_s.

The problem of radionuclide diffusion in the near-field is considered in two parts:

(i) Diffusion through the Crack

F_a, the release rate from N_c cracked canisters[4] into the bentonite, is given by:

$$F_a = \frac{2\pi r_a'' W \varepsilon_p D_p N_c C_0}{\sinh(L'')} \left[\frac{C_s}{C_0} - \cosh(L'') \right]. \qquad (31)$$

[4] It is probably unrealistic to assume that all canisters in the repository become cracked simultaneously and in the same way. This assumption is made in the absence of a detailed model of canister failure. In reality, canisters are likely to fail at different times and crack widths will be time-dependent.

The derivation of Equation (31) is given in Appendix II (Equation (II.6)). The double prime indicates non-dimensionalisation with respect to the length scale μ_c [m], given by:

$$\mu_c = \begin{cases} \left(\dfrac{D_p}{R_f \lambda}\right)^{1/2} = \mu & \text{for a bentonite - filled crack} \\ \left(\dfrac{D_0}{\lambda}\right)^{1/2} & \text{for a water - filled crack} \end{cases} . \tag{32}$$

(a single prime denotes non-dimensionalisation with respect to μ). D_0 [$m^2\ y^{-1}$] is the diffusion coefficient in water. In the present calculations, this parameter was set equal to D_p, the pore diffusion coefficient for bentonite. C_0 [M] is the radionuclide concentration at the interface between the crack and the bentonite surrounding the cracked canister (Figure 5). This concentration can be determined only after consideration of diffusion through the bentonite annulus.

(ii) Diffusion through the Bentonite Annulus

The solution of the governing equation for diffusion through the bentonite annulus is discussed in Appendix III (Equation (III.23)). F_b , the release rate from the bentonite to the host rock, is given by:

$$F_b = \frac{8\pi r_b' D \varepsilon_p D_p N_c C_0 \displaystyle\int_{\theta_0=0}^{\pi/2} \sum_{i=0}^{\infty} (-1)^i K_1(R_{-i}') \sin(\theta_i) \frac{d\theta_0}{\sin^2(\theta_0)}}{K_0(r_D') \left[1 + \dfrac{2}{K_0(r_D')} \displaystyle\sum_{i=1}^{\infty} (-1)^i K_0(2iD') \right]} . \tag{33}$$

where

$$D = r_b - r_a , \tag{34}$$

$$r_D = \frac{W}{\pi} , \tag{35}$$

$$R_{-i} = \frac{(2i+1)D}{\sin\theta_{-i}} , \tag{36}$$

and

$$\theta_{-i} = \arctan\left[(2i+1)\tan(\theta_0)\right] . \tag{37}$$

C_0 , the radionuclide concentration at the interface between the crack and the bentonite annulus, is also derived in Appendix III (Equation (III.27). It is obtained by equating the flux across the crack-bentonite interface, calculated from a solution for diffusion through the crack, with that calculated from a solution for diffusion through the bentonite annulus and is given by :

$$\frac{C_0}{C_s} = \left\{ \cosh(L'') + \frac{\mu_c K_1(r_D') \sinh(L'')}{\mu K_0(r_D') \left[1 + \frac{2}{K_0(r_D')} \sum_{i=1}^{\infty} (-1)^i K_0(2iD') \right]} \right\}^{-1} . \qquad (38)$$

The summations within the expressions in Equations (33) and (38) are truncated at a point where the incorporation of additional terms in the summations has a negligible effect on the overall result. Typically, less than 50 terms are required for convergence.

5.1.2 Computational Results

Table 5a shows the effect of crack resistance on the release of ^{79}Se for two crack widths (1 μm and 1 cm). Four model variations are considered for each crack width:

- Firstly, the failed canister provides no resistance to radionuclide transport, as in the Kristallin-I near-field model; results for this case are reproduced from Table 3.
- Secondly, release from the waste is limited by the width of the crack. The thickness of canister is, however, set to zero (although no release takes place where the canister is intact). The purpose of considering this variation is to provide comparison with the third and fourth variations, in which a realistic canister thickness is assumed. This comparison aims to establish whether the thickness of the cracked canister is an important factor in reducing radionuclide release rates to the host-rock.
- Thirdly, the canister is assigned a finite thickness and is assumed to be water-filled.
- Fourthly, the canister is assigned a finite thickness and is assumed to be filled with water-saturated bentonite or porous canister corrosion products[5].

[5]Secondary iron minerals formed during the corrosion of the canisters have a large specific surface and consequently, like bentonite, high sorption capacities. Therefore, in our model we use the same sorption constants for both materials (Table 1). For convenience, we use the term "bentonite-filled crack" for both types of infill.

Table 5a: Release of ^{79}Se from a cracked canister, calculated on the basis of successively more realistic (less conservative) assumptions. Firstly, the canister is assumed to provide no resistance to radionuclide transport after failure (data reproduced from Table 3), secondly, the crack width is taken into account, but the thickness of the canister is not, thirdly, the finite-thickness canister is assumed to be water-filled and, lastly, the crack is assumed to be bentonite-filled.

	no transport resistance (Table 3)	zero-thickness canister		water-filled crack		bentonite-filled crack	
crack width [m]	-	10^{-2}	10^{-6}	10^{-2}	10^{-6}	10^{-2}	10^{-6}
$F_a / \lambda N_0$	3.3×10^{-1}	8.2×10^{-2}	3.3×10^{-2}	7.9×10^{-2}	5.0×10^{-3}	2.7×10^{-2}	4.2×10^{-6}
$F_b / \lambda N_0$	3.2×10^{-1}	8.0×10^{-2}	3.2×10^{-2}	7.7×10^{-2}	4.9×10^{-3}	2.7×10^{-2}	4.1×10^{-6}
$F_b T_L / N_0$	4.5×10^{-1}	2.1×10^{-1}	1.1×10^{-1}	2.0×10^{-1}	2.6×10^{-2}	9.7×10^{-2}	5.1×10^{-5}

For the zero-thickness canister, total releases ($F_b\ T_L\ /\ N_0$) are somewhat reduced with respect to the case of no transport resistance and this reduction is not very sensitive to the crack width. Both the release from the crack to the bentonite and that from the bentonite to the host rock are reduced by factors of 4 and 10 for the 1 cm and 1 μm crack, respectively. These reductions are small compared to the uncertainties in near-field data.

In the case of a water-filled crack of 1 cm width, releases are very similar to those obtained in the case of zero canister thickness, indicating that little transport resistance is provided by such a crack. For a water-filled crack of 1 μm width, reductions in releases compared to the case of zero canister thickness are greater, but still relatively small: both the release from the crack to the bentonite and that from the bentonite to the host rock are reduced by a factor of 7.

A greater reduction, and a greater sensitivity to crack width, is found in the case of a bentonite-filled crack. With respect to the case of zero-canister thickness, release from the 1 cm crack to the bentonite annulus is reduced by a factor of 3, whereas release from the 1 μm bentonite-filled crack is reduced by a factor of about 8 000. About the same factors are found for the release from the bentonite to the host rock.

Table 5b: Release of ^{237}Np from a cracked canister, calculated on the basis of successively more realistic (less conservative) assumptions (see also the caption to Table 5a).

	no transport resistance (Table 3)	zero-thickness canister		water-filled crack		bentonite-filled crack	
crack width [m]	-	10^{-2}	10^{-6}	10^{-2}	10^{-6}	10^{-2}	10^{-6}
$F_a/\lambda N_0$	4.0×10^{-3}	8.8×10^{-4}	3.4×10^{-4}	8.5×10^{-4}	3.2×10^{-4}	7.1×10^{-5}	7.8×10^{-9}
$F_b/\lambda N_0$	2.7×10^{-3}	5.0×10^{-4}	2.0×10^{-4}	4.9×10^{-4}	1.8×10^{-4}	4.1×10^{-5}	4.4×10^{-9}
$F_b T_L/N_0$	1.5×10^{-2}	3.5×10^{-3}	1.6×10^{-3}	3.4×10^{-3}	1.5×10^{-3}	3.9×10^{-4}	8.3×10^{-8}

Similar trends are found for ^{237}Np, as shown in Table 5b, but with a somewhat reduced release to the host rock for a zero thickness canister (with respect to the case of no transport resistance) and an even more pronounced reduction in releases for the 1 μm bentonite-filled crack. The releases from the crack itself and to the host rock are reduced by a factor of about 40 000 with respect to the case of zero-canister thickness.

To summarise, for both example radionuclides:

- A water-filled crack provides little reduction in releases, even where the crack is as small as 1 μm;
- A bentonite-filled crack can provide a considerable reduction in releases, but this reduction is sensitive to crack width - reductions of an order of magnitude or less are found for a 1 cm crack, whereas reductions of up to 4 orders of magnitude are found for a 1 μm crack.

5.2 Diffusion of Radiolytic Oxidants into the Bentonite

After the rapid consumption of the oxygen trapped in the repository, corrosion of the steel canister will proceed under highly reducing conditions due to the large amounts of reduced iron present in the canister (NAGRA 1994b). The resultant low oxidation potentials will ensure low solubilities and high sorption constants for many redox-sensitive radionuclides. After the failure of the canister, however, oxidants will form through radiolysis of the water permeating the waste glass. These oxidants could, in principle, rapidly oxidise the reduced iron on the exposed surfaces of the failure in the canister (e.g. the crack or hole surfaces) and that occurring in bentonite minerals around

the failed area. The reducing capacity of the near-field would then be lost in the failed area and radiolytic oxidants could diffuse into the bentonite, creating domains of high solubility and reduced sorption for some redox-sensitive radionuclides[6]. The objective of this section is to assess how far these domains of high oxidation potential could spread out. In the worst case, such oxidation fronts would reach the bentonite-host rock interface, leading to higher radionuclide release rates into the host-rock than is predicted under reducing conditions.

5.2.1 Production of Oxidants by Radiolysis

As long as the canister remains intact, it acts as a radiation shield which prevents the formation of radiolysis products in the bentonite pore water. However, mechanical failure of the canister will eventually take place following weakening by corrosion (NAGRA 1994b), giving rise to radiolysis reactions in the water coming in contact with the radioactive glass. Radiolysis products could then be released to the bentonite by diffusion through the failed canister.

Radiolysis is a process of chemical decomposition induced by the irradiation of a target material with α, β or γ-rays. When water is irradiated, new chemical species are produced in amounts proportional to the dose adsorbed. Many of these species are short-lived free radicals[7], such as OH^0, H^0 and the hydrated electron (e^-_{aq}). Other species, such as H_2, are inert compared to the free radicals and should remain stable for long times. In pure water, the major primary radiolysis products are (SWALLOW 1973):

$$H_2O \xrightarrow{\alpha,\beta,\gamma-\,irradiation} e^-_{aq},\ OH,\ H,\ H_2,\ H_2O_2,\ H_3O^+. \qquad (39)$$

From the above reaction it is evident that both reductants (e^-_{aq}, H, H_2) and oxidants (OH, H_2O_2) are produced. They must be present in equivalent concentrations in agreement with the principle of conservation of electrons:

$$2G(H_2O_2) + G(OH) = 2G(H_2) + G(H) + G(e^-_{aq}), \qquad (40)$$

where G denotes the yield[8] of a particular species.

Free radicals react almost instantaneously, so that the main stable primary products of α-radiolysis are hydrogen and hydrogen peroxide. In general, the effects of β and γ-radiation can be neglected, since the overall dose rate at the glass surface will be dominated by α-decay in the time span of interest (BURNS et al. 1982a).

---

[6] The solubility of some radionuclides can increase and the sorption constants can decrease by several orders of magnitude under oxidising conditions (e.g. U, Np). See RAI et al. (1990) and WANNER (1985) for the effect on solubility. See McKINLEY and HADERMANN (1985) for the effect on sorption.

[7] Free radicals are species with an unstable electronic configuration.

[8] The yield of a species is defined as the number of molecules formed per 100 eV of energy absorbed.

The oxidation potential in the bentonite pore water can increase if, for instance, the hydrogen produced by radiolysis and steel corrosion[9] remains chemically inert and the radiolytic oxidants react readily with dissolved reductants. It is well-known that reaction of H_2 with dissolved metals is sluggish in the absence of appropriate catalysts, even under very high hydrogen pressures (see MEYER & PETERS 1927, pp. 217-218).

Another possible effect of radiolysis is *pH* reduction (BURNS et al., 1982a), which would also have important effects on radionuclide solubilities. However, since large *pH* changes occur only in the presence of air (production of nitric acid from nitrogen gas), this effect will be insignificant in a repository environment. Hence, attention is focused here on the effects of radiolytic oxidants.

5.2.2 Model Assumptions

The following model assumptions are made on the generation and transport of radiolytic oxidants:

- After canister failure, reductants and oxidants are generated on the wetted surfaces of the vitrified waste in the form of equal amounts of hydrogen and hydrogen peroxide.

- All the hydrogen is conservatively assumed to remain chemically inert, leaving behind an excess of radiolytic oxidant.

- Hydrogen peroxide is produced at a rate of 0.01 mol y^{-1} per canister (McKINLEY 1985). This estimate is based on conservative assumptions of waste geometry and canister failure time (1000 years after repository closure).

- Hydrogen peroxide dissociates rapidly to oxygen and water according to the reaction $H_2O_2 \rightarrow H_2O + 1/2\ O_2$; oxygen is thus assumed to be the only oxidant escaping from the failed canister[10].

- Radiolytic oxygen is transported instantaneously from the surface of the vitrified waste to the crack outlet. Transport resistance in the fractured glass and consumption by chemical reaction[11] are thus conservatively neglected.

---

[9] The amount of H_2 produced through radiolysis is negligible compared to that which may be generated during canister corrosion.

[10] Rapid dissociation of hydrogen peroxide is known to occur in the presence of small amounts of catalysts: typically, dissolved metal ions and suspended metal oxide particles (YAMAMOTO et al. 1985). Such catalysts will undoubtedly be present in the near-field due to the chemical complexity and heterogeneity of this environment.

[11] Normally, oxygen would be reduced by reaction with the canister corrosion products (magnetite (Fe_3O_4), ferrous hydroxides, $Fe(OH)_2$, etc.). If, as we assume, ferric minerals like goethite (FeOOH), ferrihydrite ($Fe(OH)_3$) and hematite (Fe_2O_3) coat the crack walls in an impermeable layer, reduction will not be possible and all the oxygen will reach the crack outlet.

- The Fe(II) present in the water-accessible solids along the diffusion pathway is rapidly oxidised to Fe(III) by reaction with the radiolytic oxidants escaping during the earliest stages after canister failure.

- A constant concentration of dissolved Fe(II) is maintained in the solution carrying the radiolytic oxidants, through the continuous supply of reduced iron (by diffusion) from the intact regions of canister and bentonite, and from the groundwater.

- The canister failure is assumed to take the form of a circumferential water-filled crack, with the geometrical parameters given in Figure 5.

In deriving a governing equation for the transport of radiolytic oxygen through the bentonite, the processes of diffusion, sorption on pore surfaces and the simultaneous consumption of oxygen by reaction with ferrous iron dissolved in the bentonite pore water must be considered.

5.2.3 Consumption of Oxygen in the Bentonite

As soon as the radiolytic oxygen reaches the bentonite, reduction by ferrous iron dissolved in the pore water is assumed to take place. The oxidation-reduction kinetics of the oxygen-iron(II) system is well-known and summarised in STUMM & MORGAN (1981, p. 465). At $pH > 5$, the rate of oxygen reduction is proportional to the concentration of oxygen, to the total dissolved ferrous iron concentration and to the square of free hydroxyl ion concentration. Neglecting, for the moment, the processes of diffusion and sorption[12]:

$$-4\frac{d[O_2]}{dt} = -\frac{d[Fe(II)]}{dt} = k[Fe(II)][OH^-]^2[O_2], \qquad (41)$$

where

$[O_2]$	is the concentration of oxygen in solution [M];
$[Fe(II)]$	is the total dissolved ferrous iron concentration [M];
$[OH^-]$	is the free hydroxyl ion concentration [M];
k	is the kinetic constant of the reaction [M^{-3} y^{-1}].

The hydroxyl ion concentration may be approximately expressed as a function of pH and water ionisation constant, K_w. Neglecting ionic strength effects:

---

[12]The kinetic equation defined here is based on Equation (61) in STUMM & MORGAN (1981). However, it is expressed here in terms of dissolved oxygen concentration, not as a function of the oxygen partial pressure as in the original equation (see also special note in Table 6).

$$\left[OH^-\right] \cong \frac{K_w}{\left[H^+\right]} \cong 10^{pH-pK_w}, \quad (42)$$

where pK_w = -log K_w and $K_w \cong 10^{-14}$ M^2. Substituting Equation (42) in Equation (41) and defining $C \equiv \left[O_2\right]$, the consumption of oxygen in the bentonite is described by the equation:

$$\frac{dC}{dt} = -\lambda_0 C, \quad (43)$$

where

$$\lambda_0 = \frac{1}{4} k\left[Fe(II)\right] 10^{2(pH-pK_w)}. \quad (44)$$

The concentration of oxygen thus decays exponentially, allowing an analogy to be drawn with the decay of a radionuclide. This analogy is used in deriving a transport equation in section 5.2.4, below.

It should be emphasised that Equation (41) governs only the reduction of oxygen by ferrous species in solution. In heterogeneous systems, this reaction may be catalysed by ferrous species adsorbed on oxide surfaces, as pointed out in a recent review (STUMM & SULZBERGER 1992). However, neglecting catalytic effects increases the degree of conservatism of the present model and is therefore justified for safety assessment purposes. Moreover, data on the kinetics of heterogeneous Fe(II)-O_2 reactions are difficult to apply, due to large uncertainties in parameters specifically required to describe this type of reaction (e.g. the accessible surface area, to which kinetic constants of heterogeneous reactions must be normalised).

On the other hand, the kinetics of the homogeneous reaction is well established and easier to apply in model calculations. In a recent compilation, EARY & SCHRAMKE (1990) reviewed several independent experimental investigations on the oxygenation kinetics of Fe(II) in homogeneous solutions. These data confirmed the validity of Equation (41) in a wide compositional range: the proportionality to the oxygen concentration and to the square of the hydroxyl concentration was found in 5 independent studies over pH-values ranging from ~5 to 8.4. Moreover, all kinetic constants were found to agree within one order of magnitude.

5.2.4 Diffusion of Oxygen through the Bentonite

Assuming that the *pH* and the ferrous iron concentration can be treated as constants[13], by analogy with the diffusive transport of radionuclides through bentonite (see Equation

---

[13] The assumption that pH and ferrous iron concentration are constant throughout the bentonite, though unrealistic, is acceptable for the present application as long as parameter values are conservative.

(6)), the steady-state equation governing the diffusion, sorption and consumption of oxygen in the bentonite annulus is given by:

$$\frac{d^2C}{dr'^2}+\frac{1}{r'}\frac{dC}{dr'}-C \quad = \quad 0. \tag{45}$$

In Equation (45), the prime indicates non-dimensionalisation with respect to the length scale ν [m], where ν is, by analogy with Equation (4), given by:

$$\nu = \left(\frac{D_p}{R_f \lambda_0}\right)^{1/2}. \tag{46}$$

For reasons of conservatism and due to the lack of experimental data, sorption of oxygen on bentonite is neglected, i.e. R_f is set equal to one. Combining Equations (III.10) and (III.24, the concentration at an arbitrary point $P(x,y)$ within the bentonite annulus is given by:

$$\frac{C}{C_0} = \frac{\sum_{i=-\infty}^{\infty}(-1)^i K_0(r_i')}{K_0(r_D')\,B}, \tag{47}$$

where

$$B \equiv \left[1+\frac{2}{K_0(r_D')}\sum_{i=1}^{\infty}(-1)^i K_0(2iD')\right] = \frac{C_0}{C_D}. \tag{48}$$

C_0 is the oxygen concentration at the crack-bentonite boundary and r_D, C_D, r_i are defined in Appendix III (see Equations (III.2), (III.8) and (III.25)). Equation (47) can be used to assess the penetration of the oxidation front into the bentonite if the oxygen concentration along the crack, C_0, is specified. C_0 can be determined by equating the release rate of oxygen from the crack to the bentonite (given, by analogy with the case of radionuclide transport, by Equation (III.11)) with the rate of oxygen production following α-radiolysis (see Section 5.2.5). Denoting this rate of production as S [mol. y^{-1}] and substituting Equation (III.8) in Equation (III.11):

$$S = 2\pi\, r_a' W \varepsilon_p D_p C_D \frac{K_1(r_D')}{K_0(r_D')}. \tag{49}$$

The steady-state oxygen concentration at the crack outlet, C_0, is obtained eliminating C_D through substitution of Equation (III.10) into Equation (49):

$$C_0 \quad = \quad \frac{S\,B\,K_0(r_D')}{2\pi r_a' W \varepsilon_p D_p K_1(r_D')}. \tag{50}$$

Combining Equations (50) and (47), and noting that $W = \pi\, r_D$, a final expression is obtained for the oxygen concentration as a function of the crack width and of the oxidant production rate (in which C_0 and r_D no longer appear):

$$C = \frac{S \sum_{i=-\infty}^{\infty} (-1)^i K_0(r_i')}{2\pi r_a' W \varepsilon_p D_p K_1(W'/\pi)} \quad . \tag{51}$$

5.2.5 Parameter Values

The same geometrical and transport parameter values used in the model of radionuclide transport through the cracked canister (Table 2) are employed in the model of migration of radiolytic oxidants. Input data required specifically for the latter model are listed in Table 6 and discussed below.

A critical parameter is the concentration of ferrous iron in solution. Although this concentration, which controls directly the oxygen reduction rate (Equation (41)) is not known precisely, experimental data may help in defining a reasonable concentration range for our model calculations. Groundwater-bentonite interaction experiments carried out in recent years yield iron concentrations ranging from 10^{-7} to 5×10^{-5} M (SNELLMAN et al. 1987; BATEMAN et al. 1991). A similar range (2×10^{-7} to 8×10^{-5} M) has been found in groundwaters from the crystalline basement of Northern Switzerland (PEARSON & SCHOLTIS 1993). On the base of these data, a concentration of 10^{-6} M was selected for our reference calculations. For conservative calculations we chose a Fe(II) concentration of 10^{-8} M, which is one order of magnitude less than the smallest concentration defined by the experimental data mentioned above.

A further critical parameter is the *pH*, on which the reduction rate of oxygen depends exponentially (see Equations (41) and (42)): increasing the *pH* by a single unit decreases the oxygen reduction rate by two orders of magnitude. Fortunately, the *pH* values expected in the near-field are constrained within a relatively narrow range by the buffering capacity of bentonite and waste glass. Experiments carried out in various laboratories indicate that reaction of water with borosilicate glass and/or bentonite leads to stable pH-values between 8 and 10 (BATEMAN et al. 1991, SNELLMAN et al. 1987, GODON 1988). A *pH* of 8 (the most conservative value within the indicated range) was thus selected for the model calculations.

As previously noted, the assumed oxidant production rate is based on a conservative canister failure time of 1000 years after emplacement of the waste in the repository and on the assumption that the reductants (H_2) do not react with oxygen (McKINLEY 1985). The estimated H_2O_2 production rate of 0.01 mol y^{-1} relies on α-doses calculated for representative nuclear waste glasses (see Figure 1 in BURNS et al. 1982b). The release rate of oxygen from the crack outlet, *S*, is only one half this value, since only one oxygen molecule is produced upon dissociation of two hydrogen peroxide molecules ($2\, H_2O_2 \rightarrow 2\, H_2O + O_2$).

Table 6: Parameter values specifically required to model the penetration of radiolytic oxidation fronts into the bentonite buffer. The geometrical and transport parameters are specified in Table 2.

Parameter	Symbol	Value	Dimension
Dissolved ferrous iron concentration	*[Fe(II)]*	10^{-6} / 10^{-8}	[M]
Negative logarithm of proton activity	*pH*	8	[pH units]
kinetic constant for oxygen reduction*	*k*	4.45×10^{24}	[M^{-3} y^{-1}]
Production rate of oxidant, as H_2O_2, per canister	*2S*	0.01	[mol y^{-1}]
Width of circumferential crack	*W*	0.001	[m]

**Note: the kinetic constant given in Equation (41), k, differs from the value appearing in the original equation , in which the oxidation rate of ferrous iron is expressed as a function of an equilibrium oxygen partial pressure, pO_2 (STUMM & MORGAN 1981, p.465, Equation (61)). In the present work the reaction rate is more conveniently expressed as a function of the dissolved oxygen concentration, in order to facilitate the coupling with the diffusion equation. If k* is the kinetic constant given in STUMM & MORGAN's equation (transformed to [M^{-3} y^{-1}]) and K_H is Henry's constant for the equilibrium between dissolved and gaseous oxygen (1.059×10^3 atm M^{-1} at 50 °C according to the data in PEARSON & BERNER 1991), then k=100 k* K_H. The factor of 100 takes account of the increased reaction rate at the temperature expected in the near-field (50 °C instead of 20°C, to which k* refers).*

5.2.6 Definition of a Boundary between Oxidising and Reducing Conditions

If the concentration of radiolytic oxygen is sufficiently low, its presence will not significantly affect the oxidation state of redox-sensitive radionuclides. Whenever a value can be assigned to this concentration, it can then be used to define objectively a boundary between oxidising and reducing regions of the bentonite. This method is preferred to that of defining an oxidation potential for the solution. The latter approach assumes thermodynamic equilibrium among all redox pairs present in solution, a situation which is rarely observed in complex natural solutions.

In a real situation, it is possible that some redox-sensitive nuclides will be released from the glass in the oxidised state[14]. As they migrate through the bentonite, they will come into regions progressively depleted of radiolytic oxygen; finally, these nuclides will reach oxygen-free regions of the bentonite, where they will be reduced by Fe(II) or by other reductants. Clearly, where the oxygen concentration becomes negligible compared to that of a specific redox-sensitive radionuclide, only a small fraction of the radionuclides will remain in the oxidised state; the major part will be reduced by the reductants present in excess in the oxygen-free domains. Table 3.7.3 in NAGRA 1994b shows that the redox-sensitive nuclide with the *lowest* solubility is Np (10^{-10} M). Thus, in regions with an oxygen concentration of 10^{-12} M or less a maximum of 4% of the dissolved Np could be left oxidised as Np(V) and a maximum of 2% as Np(VI)[15]. The net solubility of Np will then be determined by that of Np(IV) in regions with oxygen concentrations of less than 10^{-12} M and by that of oxidised Np forms in regions of higher oxygen concentrations. The same limit of 10^{-12} M has been conservatively adopted for the other (more soluble) redox-sensitive nuclides.

5.2.7 Computational Results

The results of the model calculations performed using the parameter values discussed above are presented in Figure 6, which shows the distribution of radiolytic oxygen in an axial cross-section through the repository. The contours are isopleths (lines of uniform concentration) representing the loci of 10^{-12} M dissolved oxygen concentration. The isopleths were calculated for two Fe(II) concentrations (10^{-6} and 10^{-8} M) and two oxidant production rates. Inside the contours steady-state oxygen concentrations exceed 10^{-12} M, while outside the contours lower concentrations prevail. The value of 10^{-12} M is the limit separating oxidising from reducing regions in the bentonite. This value is related to the solubility of redox-sensitive radionuclides, as explained in section 5.2.6.

Figure 6 shows that the penetration of the radiolytic oxidation front in the bentonite is predicted to be insignificant even assuming the unusually low Fe(II) concentrations of 10^{-8} M. Using the oxidant production rate indicated in Table 6, penetration depths of 2 mm and 1.5 cm are calculated for Fe(II) background concentrations of 10^{-6} M and 10^{-8} M, respectively (solid lines). Such penetration depths are less than about 1% of the bentonite thickness. As a further parameter variation, a calculation has been performed for an oxidant production rate increased by a factor of 40, which represents the case of early water access into a mis-sealed canister[16]. The results (broken lines) indicate a very

---

[14] Besides the fact that many nuclides held in the glass may lie from the beginning in the oxidised state, there will be enough radiolytic oxidant in the pore water permeating the waste glass to oxidise all redox-sensitive nuclides before they reach the crack outlet.

[15] The figure of 4% arises from the fact that a single oxygen molecule can oxidise 4 Np(IV) cations to Np(V).

[16] The factor of 40 is obtained from the empirical formula given by McKINLEY (1985, p.93) assuming water ingress 1 year after emplacement of the waste. This assumption is exceedingly conservative, but the aim of this calculation was merely to assess the sensitivity of the results to large variations of the oxidant production rate.

small displacement in the position of the 10^{-12} M oxygen isopleths in spite of the large increase in the oxidant production rate. The displacements are 4 mm and less than 1 mm assuming background Fe(II) concentrations of 10^{-8} M and 10^{-6} M, respectively. This insensitivity can be explained with the help of the simplified equations presented in Appendix IV.

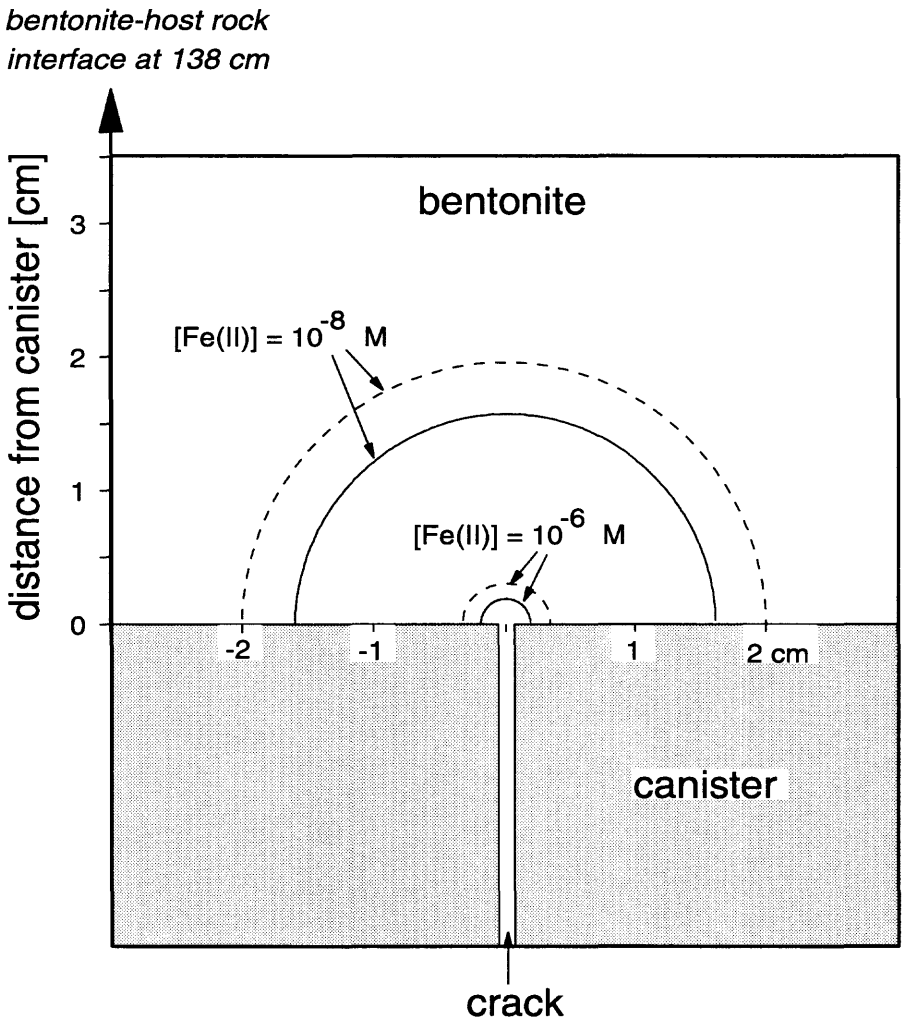

Figure 6: Penetration of the radiolytic oxidation front, defined by 10^{-12} M contours of dissolved oxygen. Calculations are shown for two background concentrations of ferrous iron in the bentonite pore water (10^{-6} and 10^{-8} M). Solid lines refer to calculations performed with the parameter values given in Tables 2 and 6. Broken lines show the effect of increasing the oxidant production rate by a factor of 40.

Under realistic conditions, therefore, the production of radiolytic oxidants will not affect the redox state of oxidisable nuclides beyond a very small region around the crack. In the worst case, regions with enhanced radionuclide solubility would penetrate about 2 cm into the bentonite and the performance of the near-field would not be compromised.

Only in one extreme case the formation of radiolytic oxidants could have serious consequences on the near-field performance: if a cracked canister sinks completely through the bentonite, so that the waste package comes in contact with the host rock, a small part of the circumferential crack would release oxidised radionuclides directly into the geosphere. In this case, however, other processes, related to the loss of beneficial properties of the bentonite as a barrier (e.g. colloid filtration), would become more important. As discussed in chapter 4.1, the possibility of complete canister sinking appears very unlikely.

The effect of oxidation fronts on the release rate of redox-sensitive radionuclides to the host rock can be in principle evaluated if, in the model calculations, the thickness of the bentonite buffer is reduced by an amount equal to the penetration depth of the oxidation front. Parameter variations performed in the context of the Kristallin-I safety analysis (CURTI 1995) indicate that even a large reduction of the bentonite thickness (from 1.38 to 0.2 m) would have limited consequences on the peak radionuclide release rates to the host rock, which would increase usually by less than a factor of 10. A decrease of the bentonite thickness from 1.38 to 1 m increases the peak release rate of ^{135}Cs by less than 30%. From these figures, it is clear that reducing the bentonite thickness by only 1.5 cm (the maximum predicted extension of the oxidation front) will have a negligible effect on the resultant release rates.

5.2.8 Comparison with the Model of Romero et al.

Recently, ROMERO et al. (1995) developed a model on the formation and movement of radiolytic oxidation fronts for the Swedish high-level waste repository. Their approach differs from that used in this report in some important aspects, partly as a consequence of fundamental differences in the design of the Swedish and Swiss repositories.

The mentioned model defines the advancing redox front as a boundary separating regions where the Fe(II) in the bentonite (or in the host rock) has been completely oxidised by the radiolytic oxidants from those where the iron is still in reduced form. With this approach, it is implicitly assumed that the Fe(II) concentration in the pore water within the oxidised domain of the bentonite is insignificant. This assumption may be reasonable for the Swedish repository concept, in which the use of iron-based materials is not foreseen, but cannot be applied to the Swiss repository, where massive steel canisters and, to a lesser extent, the unoxidised bentonite and groundwater, will act as an effectively inexhaustible reservoir of ferrous iron to the pore solution.

In our approach, we conservatively assume a rapid oxidation of the ferrous iron in the solid phases in and around the failure zone, and then focus on the Fe(II)-oxygen reaction *in solution* to predict the migration of radiolytic oxidants in the bentonite. The kinetics of this reaction is well established and thus suitable for quantitative calculations. Romero et al., on the other hand, neglect (conservatively) the effects of dissolved Fe(II). They consider instead the reduction of radiolytic oxidants by ferrous iron in the solids,

implicitly assuming an *instantaneous* kinetics for the reaction between hydrogen peroxide and ferrous iron. The latter assumption is, however, non-conservative: if this reaction is slow enough (i.e. if the reaction rate happens to be in the range of the oxidant transport times), then the redox front would travel faster than predicted by their model. This effect may be relevant for those calculations which assume high radiolysis rates and low Fe(II) contents. A further assumption made by Romero et al. is that *all* the ferrous iron available in the bentonite reacts with the oxidants. In reality, a substantial part of the Fe(II) in the bentonite may be "locked" within octahedral sites of clay minerals. If these minerals remain thermodynamically stable and do not dissolve during the interaction with radiolysis products, this iron might remain inaccessible to the radiolytic oxidants.

5.2.9 The Influence of Oxidants Dissolved from the Waste Glass

Borosilicate glasses for the vitrification of high-level waste in Switzerland contain redox-sensitive elements, either radionuclides (i.e. isotopes of U, Np, Se) or inactive elements (mainly Fe). Because there are no data on the oxidation state of redox-sensitive elements in these glasses, the possibility must be considered that a significant fraction of these elements are in an oxidised form. Assuming full oxidation of these elements in the waste, it is possible to estimate a pessimistic release rate of non-radiolytic oxidants from the dissolving glass and then compare this number with the production rate of radiolytic oxidants assumed in our model.

Our calculations indicate that, even assuming a fast glass corrosion rate, the oxidants released from the glass would correspond, on an electron equivalent basis, only to a small fraction of the oxidants released by water radiolysis. Assuming complete oxidation of Fe and Se in the glass (to ferric iron and selenate), both elements together would contribute less than 10% of the oxidants assumed to be produced by water radiolysis. Since the combined oxidising capacity of the other redox sensitive elements in the glass is negligible compared to that of ferric iron and selenate together, it can be concluded that the total release rate of oxidants from the glass at the time of canister failure should not exceed the rate of production of radiolytic oxidants. It seems therefore unlikely that non-radiolytic oxidants released from the glass could significantly increase the penetration depth of an oxidation front in the bentonite.

6 Summary and Conclusions

An investigation of the effects of a limited number of processes, considered negligible and thus neglected in the Kristallin-I near-field performance assessment, has been carried out. These processes have been excluded from the Kristallin-I near-field model, either because they were thought unlikely to occur to a significant degree, or because they are likely to make a positive contribution to the performance of the near-field as a barrier to radionuclide migration (i.e. neglecting them is conservative), but are insufficiently understood to justify incorporating them in a model to be used in a safety assessment. The aim of this report was to investigate, by means of a set of simple, steady-state models, whether the arguments for neglecting these processes in the near-field model assumptions of Kristallin-I can be justified.

The following processes and their consequences on the release of radionuclides to the geosphere were examined:

– Back-diffusion of radionuclides from the host rock to the bentonite.

– Sinking of the waste packages through the bentonite buffer due to creep deformation.

– Transport resistance through a circumferential crack in the canister.

– Migration of radiolytic oxidants emerging from a circumferential crack in the canister.

In the case of back-diffusion of radionuclides from the host rock to the bentonite, it was found that neglecting this process, by setting the radionuclide concentration at the outer bentonite boundary equal to zero, may have a large effect on the total release to the host rock. A zero-concentration boundary condition at the bentonite-host rock interface can thus result in an over-estimation of release by about an order of magnitude for the chosen reference radionuclides ^{237}Np and ^{79}Se. Therefore, the use of a "mixing-tank" boundary condition in the Kristallin-I Reference Case, which considers the effects of back-diffusion through the assumption of a finite groundwater flowrate past the repository, is justified.

In the case of canister sinking within the bentonite, although in reality only small displacements are expected, steady-state calculations indicate that even fairly large displacements would have little effect on the net release of radionuclides to the host rock, which would increase by less than 20 % for a canister sinking half-way to the tunnel floor. This indicates that neglecting canister settlement in the calculation of radionuclide releases from the near-field is unlikely to result in significant underestimates of radiological consequences, even if the degree of settlement is far greater than expected.

Finally, in the case of localised canister failure, steady-state calculations for a bentonite-filled crack indicate that the transport resistance of the crack reduces radionuclide releases by up to an order of magnitude for a 1 cm thick crack and by more than four orders of magnitude for a 1 μm crack. This indicates that, although it is difficult to

bound the likely dimensions of any cracks or holes in the canister following failure, neglecting the transport resistance of such openings gives results which err greatly on the side of conservatism. The transport resistance would nevertheless be considerably weaker in the (unlikely) case of a crack which is filled with water. Then, the radionuclide release rates to the geosphere of the selected example nuclides would be only one to two orders of magnitude less than those calculated using the Kristallin-I model (Reference Case).

Calculations indicate that oxidants produced by radiolysis within the waste package should not penetrate significantly into the bentonite under the conditions expected. Even with highly conservative assumptions concerning the time of canister failure, the oxidant production rate and the rate of transport of oxidants to the crack outlet, the redox front would penetrate less than 2 cm into the bentonite. This means that, under normal conditions, regions of enhanced radionuclide solubility and reduced sorption would be confined to very small domains far away from the bentonite-host rock boundary. Therefore it is very unlikely that the formation of radiolytic oxidants will enhance the release of redox-sensitive radionuclides into the host rock.

In conclusion, the calculations performed in this study provide justification for certain assumptions made within the Kristallin-I near-field model. Processes neglected in making these assumptions are likely either to reduce radionuclide releases (diffusion of radionuclides from the host rock to the bentonite; transport resistance of a failed canister) or to have very little effect on radionuclide releases (creep deformation within the bentonite, migration of radiolytic oxidants from a locally breached canister).

Appendix I - Radionuclide Concentration Distribution for a Displaced Canister

(i) Separable Solution of the Diffusion Equation

Radionuclide diffusion through the bentonite is described by Equation (6):

$$\frac{1}{r'^2}\frac{\partial^2 C}{\partial \alpha^2}+\frac{1}{r'}\frac{\partial}{\partial r'}\left(r'\frac{\partial C}{\partial r'}\right)-C=0. \tag{I.1}$$

In order to obtain a solution to this equation appropriate to the geometry shown in Figure 3 (the case of a canister displaced through a distance d from the centre of the emplacement tunnel) the method of separation of variables is employed (see, for example, chapter 10 in RILEY 1974). Solutions of the governing partial differential equation are sought that have the form:

$$\frac{C_{\lambda_i}(\alpha,r')}{C_s}=U_{\lambda_i}(\alpha)R_{\lambda_i}(r'), \tag{I.2}$$

where $C=C_{\lambda_i}$ is a solution obtained by assigning the separation constant the value λ_i. Substituting Equation (I.2) in Equation (I.1) and rearranging in order to separate terms into those which are functions of α and those which are functions of r' leads to:

$$\frac{r'}{R_{\lambda_i}}\frac{\partial}{\partial r'}\left(r'\frac{\partial R_{\lambda_i}}{\partial r'}\right)-r'^2=-\frac{1}{U_{\lambda_i}}\frac{\partial^2 U_{\lambda_i}}{\partial \alpha^2}=\lambda_i. \tag{I.3}$$

where λ_i must be a constant (since it is a function of α only and a function of r' only). Since Equation (I.1) is linear, a linear combination of solutions is also a solution. Therefore, the solution that satisfies both this equation and the boundary conditions is sought in the form:

$$\frac{C_{\lambda_i}(\alpha,r')}{C_s}=\sum_i c_i\, U_{\lambda_i}(\alpha)\; R_{\lambda_i}(r') \tag{I.4}$$

where the separation constants λ_i and the coefficients c_i are chosen to satisfy the boundary conditions (i.e. a fixed concentration C_s at the glass-bentonite interface and a zero concentration at the bentonite-host rock interface).

Solutions to the equation:

$$-\frac{1}{U_{\lambda_i}}\frac{\partial^2 U_{\lambda_i}}{\partial \alpha^2}=\lambda_i \tag{I.5}$$

take the form:

$$U_{\lambda_i}(\alpha) = p_i \cos\left(\alpha\sqrt{\lambda_i}\right) + q_i \sin\left(\alpha\sqrt{\lambda_i}\right), \tag{I.6}$$

where p_i and q_i are constants. Referring to Figure 3, the symmetry of the system requires that:

$$U_{\lambda_i}(\alpha) = U_{\lambda_i}(-\alpha), \tag{I.7}$$

and

$$U_{\lambda_i}(\alpha) = U_{\lambda_i}(\alpha + 2\pi). \tag{I.8}$$

In order to satisfy Equation (I.7),

$$q_i = 0 \tag{I.9}$$

and, in order to satisfy Equation (I.8), $\sqrt{\lambda_i}$ must be an integer:

$$\sqrt{\lambda_i} = i. \tag{I.10}$$

Thus, from Equation (I.6),

$$U_{\lambda_i}(\alpha) = p_i \cos(i\alpha). \tag{I.11}$$

Substitution of Equation (I.11) in Equation (I.4) yields the modified Bessel equation:

$$r' \frac{\partial}{\partial r'}\left(r' \frac{\partial R_{\lambda_i}}{\partial r'}\right) - R_{\lambda_i}\left(r'^2 + i^2\right) = r'^2 \frac{\partial^2 R_{\lambda_i}}{\partial r'^2} + r' \frac{\partial R_{\lambda_i}}{\partial r'} - R_{\lambda_i}\left(r'^2 + i^2\right) = 0, \tag{I.12}$$

which has solutions of the form:

$$R_{\lambda_i}(r') = u_i I_i(r') + v_i K_i(r'), \tag{I.13}$$

where u_i and v_i are further constants and $I_i(r')$ and $K_i(r')$ are modified Bessel functions of order i (see, for example, Ch 9.6 in ABRAMOWITZ & STEGUN 1970).

Substituting Equation (I.11) and Equation (I.13) in Equation (I.3), the concentration in the bentonite is given by:

$$\frac{C(\alpha, r')}{C_s} = \sum_i \cos(i\alpha)\left[a_i I_i(r') + b_i K_i(r')\right], \tag{I.14}$$

where the constants a_i and b_i are related to the earlier defined constants by:

$$a_i = p_i\, u_i \tag{I.15}$$

and

$$b_i = p_i\, \nu_i . \tag{I.16}$$

(ii) Boundary Conditions

These constants are fixed in such a way that the boundary conditions at the inner and outer surfaces of the bentonite are satisfied. This is possible because the cosine terms in Equation (I.14) form a complete set of mutually orthogonal functions (see p.283 in RILEY 1974).

Along the glass-bentonite interface, a concentration C_s is imposed. From Equation (I.14):

$$1 = \sum_i \cos(i\alpha)\left[a_i I_i^a + b_i K_i^a\right], \tag{I.17}$$

where the following notation is adopted:

$$I_i^a \equiv I_i(r_a') \tag{I.18}$$

and

$$K_i^a \equiv K_i(r_a'). \tag{I.19}$$

Multiplying both sides of Equation (I.17) by $\cos(j\alpha)$, where α is an integer, integrating from $\alpha = 0$ to $\alpha = 2\pi$, and using the orthogonality of the cosine terms, i.e. that:

$$\int_0^{2\pi} \cos(i\alpha)\cos(j\alpha)\,d\alpha = \begin{cases} 0 & \text{for i} \neq \text{ j} \\ \pi & \text{for i} = \text{j} \neq 0 \end{cases} \tag{I.20}$$

the following equation is obtained:

$$0 = a_i I_i^a + b_i K_i^a; \qquad i \neq 0 \tag{I.21}$$

Substituting Equation (I.21) in Equation (I.17), all terms in the summation on the right-hand side are equal to zero, except that corresponding to $i = 0$. Thus,

$$1 = a_0 I_0^a + b_0 K_0^a . \tag{I.22}$$

Along the bentonite-host rock interface, a zero concentration is imposed. In practice, the summation in Equation (I.14) is truncated and the boundary condition is satisfied exactly at a limited number $(m+1)$ of points distributed around the boundary. The points are evenly spaced in α and have coordinates (r_j, α_j), where:

$$r_j = \sqrt{r_b^2 - d^2 \sin^2(\alpha_j)} - d\cos(\alpha_j); \quad \begin{cases} j = 0,1,\ldots,m \\ \alpha_j = \dfrac{j\pi}{m} \end{cases} . \tag{I.23}$$

From Equation (I.14), at these points:

$$0 = \sum_{i=0}^{m} c_i^j \left(a_i I_i^j + b_i K_i^j\right), \tag{I.24}$$

where:

$$c_i^j \equiv \cos(i\alpha_j), \tag{I.25}$$

$$I_i^j \equiv I_i(r_j'), \tag{I.26}$$

$$K_i^j \equiv K_i(r_j'), \tag{I.27}$$

Equations (I.21), (I.22) and (I.24) can be combined to form a single matrix equation, which must be solved in order to evaluate the unknown constants a_i and b_i :

$$\begin{bmatrix} I_0^a & K_0^a & 0 & 0 & 0 & 0 & \ldots \\ 0 & 0 & I_1^a & K_1^a & 0 & 0 & \ldots \\ 0 & 0 & 0 & 0 & I_2^a & K_2^a & \ldots \\ \vdots & & & & & & \\ I_0^0 c_0^0 & K_0^0 c_0^0 & I_1^0 c_1^0 & K_1^0 c_1^0 & I_2^0 c_2^0 & K_2^0 c_2^0 & \ldots \\ \vdots & & & & & & \\ I_0^m c_0^m & K_0^m c_0^m & I_1^m c_1^m & K_1^m c_1^m & I_2^m c_2^m & K_2^m c_2^m & \ldots \end{bmatrix} \begin{bmatrix} a_0 \\ b_0 \\ a_1 \\ b_1 \\ \vdots \\ a_m \\ b_m \end{bmatrix} = \begin{bmatrix} 1 \\ 0 \\ 0 \\ 0 \\ \vdots \\ 0 \\ 0 \end{bmatrix} . \tag{I.28}$$

Equation (I.28) is solved for a_i and b_i using the MATH/LIBRARY of IMSL, Inc. (IMSL, 1989) for a range of values of canister displacement d. It has been found that, for canister displacements of up to 50% ($d = \frac{r_b - r_a}{2}$; i.e. with the canister displaced half way from the centre of the tunnel to the tunnel floor), a close approximation to the required boundary conditions can be achieved by fixing them exactly at only a small number of points ($m = 3$; i.e. 4 points). For larger displacements, more points are required to achieve a similarly close approximation. It has been found impossible to invert the matrix on the left-hand side of Equation (I.28) for canister displacements above about 60%, while including a sufficient number of points to give a reasonable approximation to the boundary conditions.

Appendix II - Release Rate from a Cracked Canister

A Cartesian coordinate system is adopted for modelling diffusion through the crack, with its origin at the centre of the crack on the canister-bentonite interface. The x-axis is parallel to the axis of the waste package, the y-axis is normal to the plane of the interface and the z-axis lies along the crack. The curvature of the crack is neglected. This simplified model of the crack is illustrated in Figure II.1. From Equation (1), one-dimensional steady-state radionuclide diffusion and decay in the crack is described by the equation:

$$\frac{\partial^2 C}{\partial y''^2} - C = 0 . \qquad \text{(II.1)}$$

where the double prime indicates non-dimensionalisation with respect to the length scale μ_c [m], defined in Equation (32).

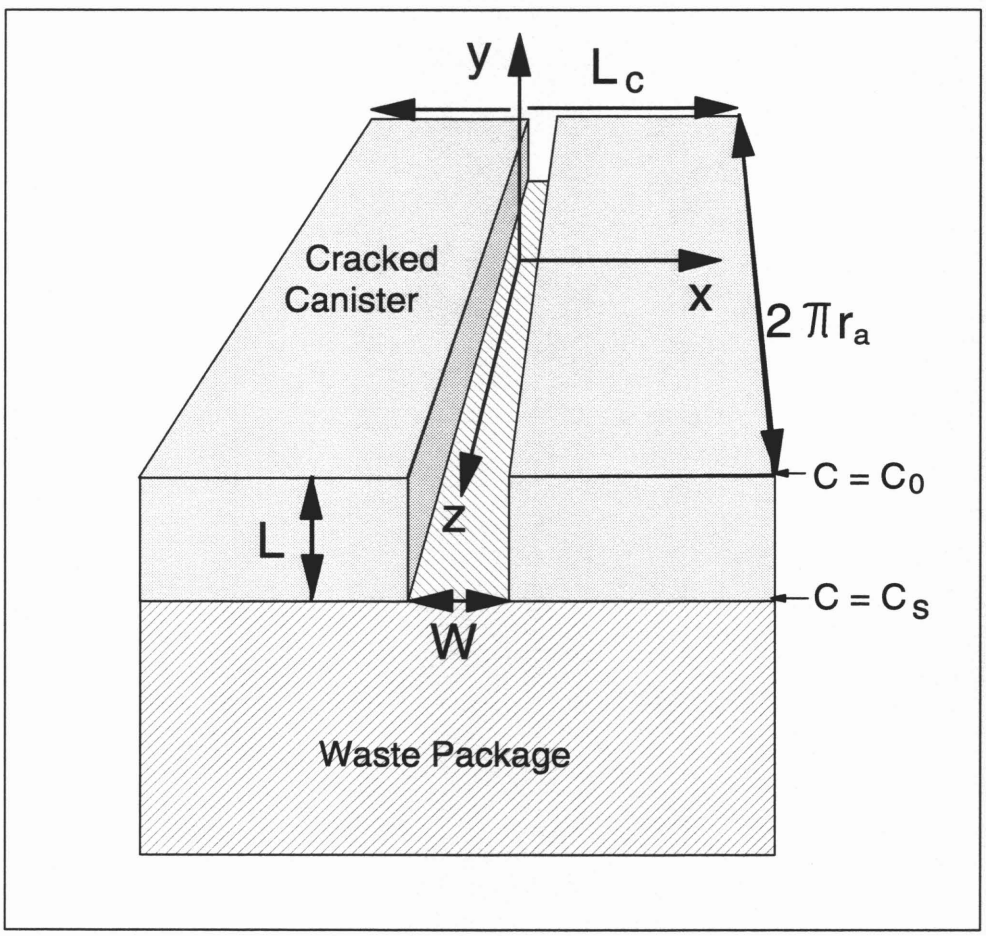

Figure II.1: The system of coordinates used in the modelling of radionuclide release from a cracked canister.

The radionuclide concentration at the origin is C_0, the value of which is initially unknown and is determined by ensuring that radionuclide flux is continuous across the boundary between the crack and the surrounding bentonite annulus (see Appendix III). The concentration at the inner surface of the canister is C_s , which is the solubility limit. The boundary conditions for Equation (II.1) are therefore:

$$C = C_0 \qquad \text{when} \qquad y'' = 0 \tag{II.2}$$

and

$$C = C_s \qquad \text{when} \qquad y'' = -L''. \tag{II.3}$$

The solution is given by:

$$\frac{C}{C_0} = -\frac{1}{\sinh L''}\left[\frac{C_s}{C_0}\sinh y'' - \sinh(L'' + y'')\right] \tag{II.4}$$

The release rate from N_c cracked canisters into the bentonite is given by:

$$F_a = -2\pi r_a'' W \varepsilon_p D_p N_c \frac{\partial C}{\partial y''}\Big|_{y''=0} . \tag{II.5}$$

Differentiating Equation (II.4), with boundary conditions (II.2) and (II.3), and substituting the result in Equation (II.5):

$$F_a = \frac{2\pi r_a'' W \varepsilon_p D_p N_c C_0}{\sinh(L'')}\left[\frac{C_s}{C_0} - \cosh(L'')\right], \tag{II.6}$$

Appendix III - Release Rate from the Bentonite Annulus

A polar coordinate system (r,θ,z) is adopted for modelling diffusion through the bentonite annulus, with its origin coinciding with that of the Cartesian coordinates (x,y,z) employed in Appendix II for modelling diffusion through the crack (Figure III.1). Also in this case, the curvature of the bentonite annulus is neglected; i.e. $C = C(r',\theta)$. From Equation (1), in the coordinate system (r',θ), steady-state radionuclide diffusion and decay in the bentonite annulus is described by the equation:

$$\frac{1}{r'^2}\frac{\partial^2 C}{\partial \theta^2}+\frac{1}{r'}\frac{\partial}{\partial r'}\left(r'\frac{\partial C}{\partial r'}\right)-C=0. \qquad \text{(III.1)}$$

In order to simplify the solution of the diffusion equation within the bentonite, the interface between the crack and the bentonite is assumed to lie along a surface of semi-circular cross-section, with radius r_D (Figure III.1), where:

$$r_D=\frac{W}{\pi}. \qquad \text{(III.2)}$$

The perimeter of the semi-circle is therefore equal to the crack width. The radionuclide concentration along this interface is C_0 , the value of which is initially unknown and is determined by ensuring that solutions for radionuclide flux out of the crack (see Appendix II) and into the bentonite annulus is continuous across the interface. Across the intact canister surface, the radionuclide flux, and thus the normally-directed concentration gradient, is zero. The boundary conditions for diffusion are therefore:

$$C = C_0 \quad \text{for} \quad r = r_D, \quad 0 \le \theta \le \pi, \qquad \text{(III.3)}$$

$$\frac{\partial C}{\partial \theta}=0 \quad \text{for} \quad r > r_D, \quad \theta = 0,\pi \qquad \text{(III.4)}$$

and

$$C=0 \quad \text{for} \quad y=D. \qquad \text{(III.5)}$$

D [m] is the thickness of the bentonite annulus:

$$D=r_b-r_a. \qquad \text{(III.6)}$$

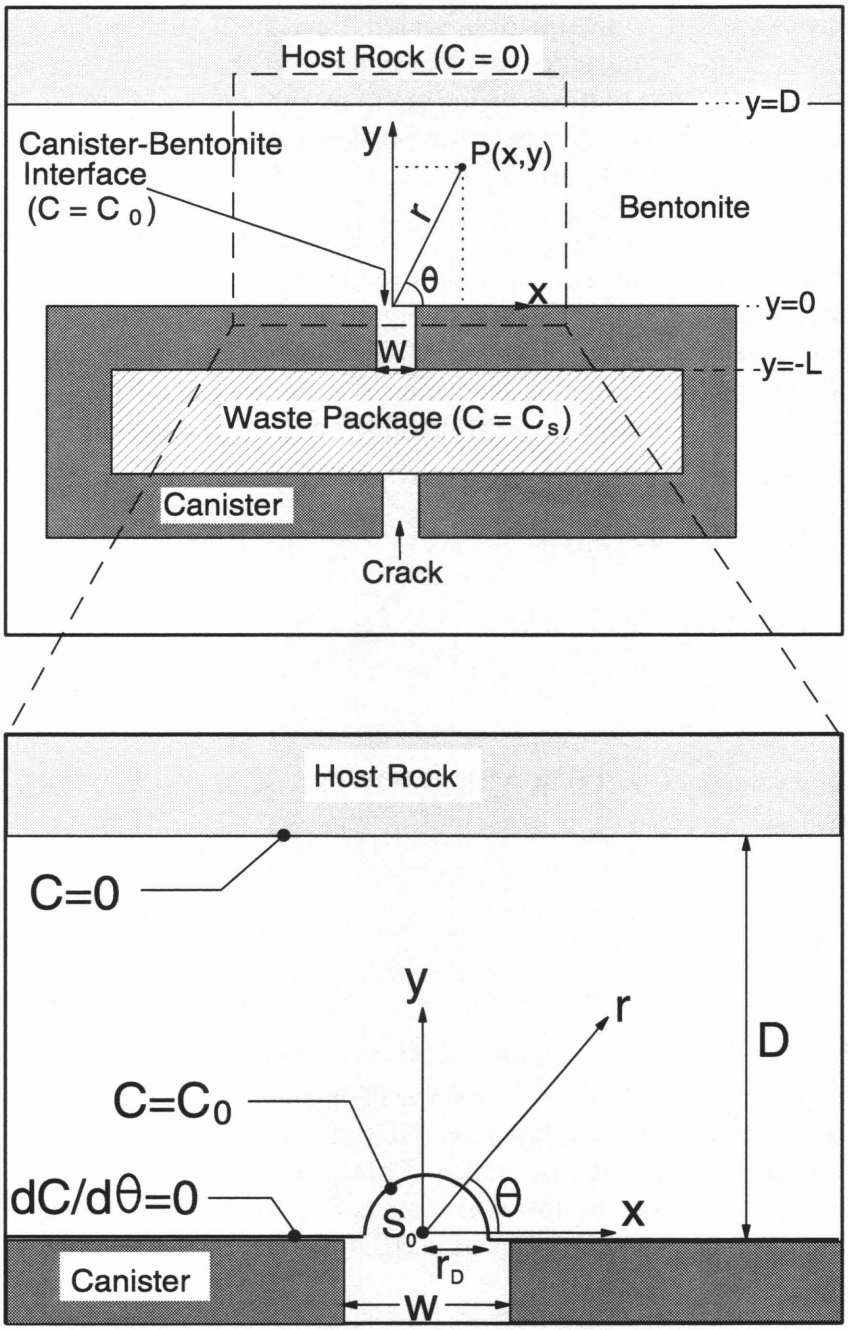

Figure III.1: The system of coordinates and the boundary conditions used in the modelling of radionuclide and radiolytic oxidant diffusion through the bentonite annulus. The z-axis lies perpendicular to the drawing plane.

Since the diffusion equation (Equation (III.1)) is linear, it is possible to use a superposition method (the method of images) to solve the problem, whereby a number of solutions to the diffusion equation, which individually do not necessarily satisfy the boundary conditions, are added together in order to obtain a solution which does satisfy these conditions. The solutions which are to be superimposed are those for a number of hypothetical line-sources of mass, distributed in such a way that the boundary conditions (Equations (III.3) - (III.5)) are satisfied.

The first of these mass sources, denoted as S_0, lies along the z-axis of the polar coordinate system $(0,0,z)$, as shown in Figure III.1. Considering the general solution of the modified Bessel function (given by Equation I.13) and noting that a solution is required that tends to zero at large distances from the source, the solutions to Equation (III.1) for the concentration C_{S_0} [M] and its gradient at a non-dimensional distance r' from the source are, in the absence of physical boundaries:

$$\frac{C_{S_0}(r')}{C_D} = \frac{K_0(r')}{K_0\left(r_D'\right)} \tag{III.7}$$

(see, for example, Ch. 9.6 in ABRAMOWITZ & STEGUN 1970). Differentiating Equation (III.7),

$$\frac{1}{C_D}\frac{dC_{S_0}}{dr'} = -\frac{K_1(r')}{K_0(r_D')}. \tag{III.8}$$

C_D [M] is the (as yet to be determined) concentration due to this hypothetical source at a distance r_D' from the source. This is not generally equal to the concentration C_0 required by the boundary condition of Equation (III.3); the zero-concentration boundary condition at the bentonite-host rock interface (Equation (III.5)) is also not satisfied[17]. The symmetry of the solution, however, means that the boundary condition of zero flux across the intact canister wall (Equation (III.4)) is met by this solution.

The additional (image) mass sources, the concentrations due to which are superimposed in order to obtain a solution which satisfies all the boundary conditions, are denoted as S_1, S_{-1}, S_2, S_{-2}, S_3, S_{-3}, ..., as illustrated in Figure III.2. The concentration within the bentonite annulus is then given by:

---

[17]The required boundary condition will be satisfied by the *superposition* of the different solutions. Equations (III.7) and (III.8) are two particular solutions of an ideally infinite number of solutions to be superposed, hence C_D generally differs from C_0.

$$C = \sum_{i=-\infty}^{\infty} C_{S_i} . \qquad \text{(III.9)}$$

The image S_1 is of equal strength but opposite in sign to S_0 and, in the polar coordinate system, is located along the line ($2D$, π, z). S_1 is a source of "negative mass" - which, although not a physically meaningful concept, is a convenient mathematical device introduced in order to satisfy boundary conditions. Since S_0 and S_1 are oppositely signed and equally distant from the bentonite-host rock interface, their contributions to concentration at the interface cancel and the boundary condition of Equation (III.5) is met. However, the concentration at the crack-bentonite interface is modified by S_1, thus violating the boundary condition of zero flux across the intact canister wall (Equation (III.4)).

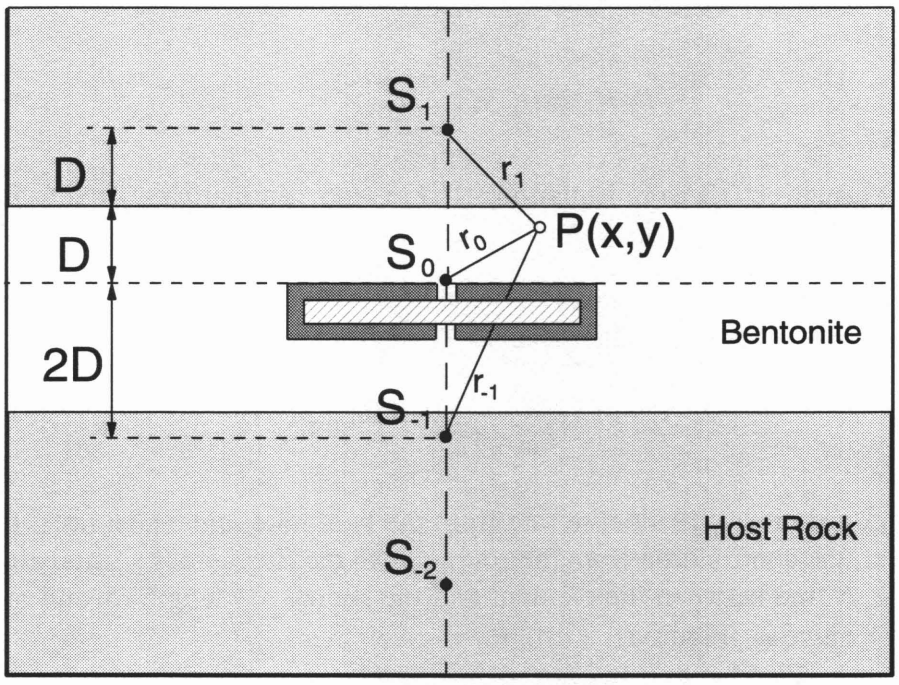

Figure III.2: The system of image line sources used to satisfy the boundary conditions.

Therefore a further image S_{-1} is introduced along the line ($-2D$, π, z); this has the same sign as S_1, and cancels the flux due to S_1 across the canister wall. S_{-1} violates the boundary condition at the bentonite-host rock interface, as was the case when S_0 was considered in isolation. However, because S_{-1} is more distant from this interface than is the case for S_0, a closer approximation to the required boundary condition is achieved.

A set of image sources extending to infinity in both the positive and negative y-directions is generated in this way, and the boundary conditions are asymptotically

approached. Each image gives a contribution to the concentration at the interface between the crack and the bentonite; the total concentration due to all images should equal C_0 in order to satisfy the boundary condition of Equation (III.3). The contribution due to source S_0 is C_D . That due to source S_1 is negative, since this source is oppositely signed, and, from Equation (III.7), is equal to $-K_0(2D')/K_0(r_D')$ .This is an approximation, in which it is assumed that the crack is sufficiently narrow (with respect to D) that the contribution due to S_1 (and to the other image sources) varies negligibly from point to point on the (semi-circular) crack-bentonite interface: $2D >> r_D$. Summing the contributions to C_0 from all sources:

$$\frac{C_0}{C_D} = 1 + \frac{2}{K_0(r_D')} \sum_{i=1}^{\infty} (-1)^i K_0(2iD'). \qquad \text{(III.10)}$$

The source S_0 is the only source contributing to the release rate from the crack to the bentonite annulus. The contribution from S_1 is cancelled by the contribution from S_{-1}. Similarly, those of S_2 and to S_{-2} cancel, etc. The release rate from the crack is therefore given by:

$$F_a = -2\pi\, r_a'\, W \varepsilon_p\, D_p \left. \frac{dC_{S_0}}{dr'} \right|_{r'=r_D'} . \qquad \text{(III.11)}$$

Substituting Equation (III.8) in Equation (III.11), and eliminating C_D using Equation (III.10)

$$F_a = \frac{2\pi\, r_a' W \varepsilon_p D_p C_0\, K_1(r_D')}{K_0(r_D') \left[1 + \frac{2}{K_0(r_D')} \sum_{i=1}^{\infty} (-1)^i K_0(2iD') \right]} . \qquad \text{(III.12)}$$

All sources contribute to the release rate from the bentonite to the host rock. Consider first, however, the contribution from the source S_0 to the flux across a small element of the interface. A line between the element and the source has length R_0 and meets the interface at an angle θ_0 (Figure III.3 (a)). R_0 is given by:

$$R_0 = \frac{D}{\sin\theta_0} . \qquad \text{(III.13)}$$

The element subtends an angle $\delta\theta_0$ at the source, so that the length of the element parallel to the tunnel axis is $R_0\delta\theta_0 / \sin\theta_0$. The element is assigned a width equal to the circumference of the tunnel, $2\pi r_b$, and therefore has an area, δA [m^2], equal to the product of its length and width: $2\pi r_b R_0 \delta\theta_0 / \sin\theta_0 = 2\pi r_b D \delta\theta_0 / \sin^2\theta_0$ .The normal component of the flux at the position of the element due to the source S_0, $f_{b,0}$ [mol m^2 y^{-1}], is given by:

$$f_{b,0} = -\varepsilon_p D_p \left. \frac{dC_{S_0}}{dr} \right|_{r=R_0} \sin\theta_0 . \qquad \text{(III.14)}$$

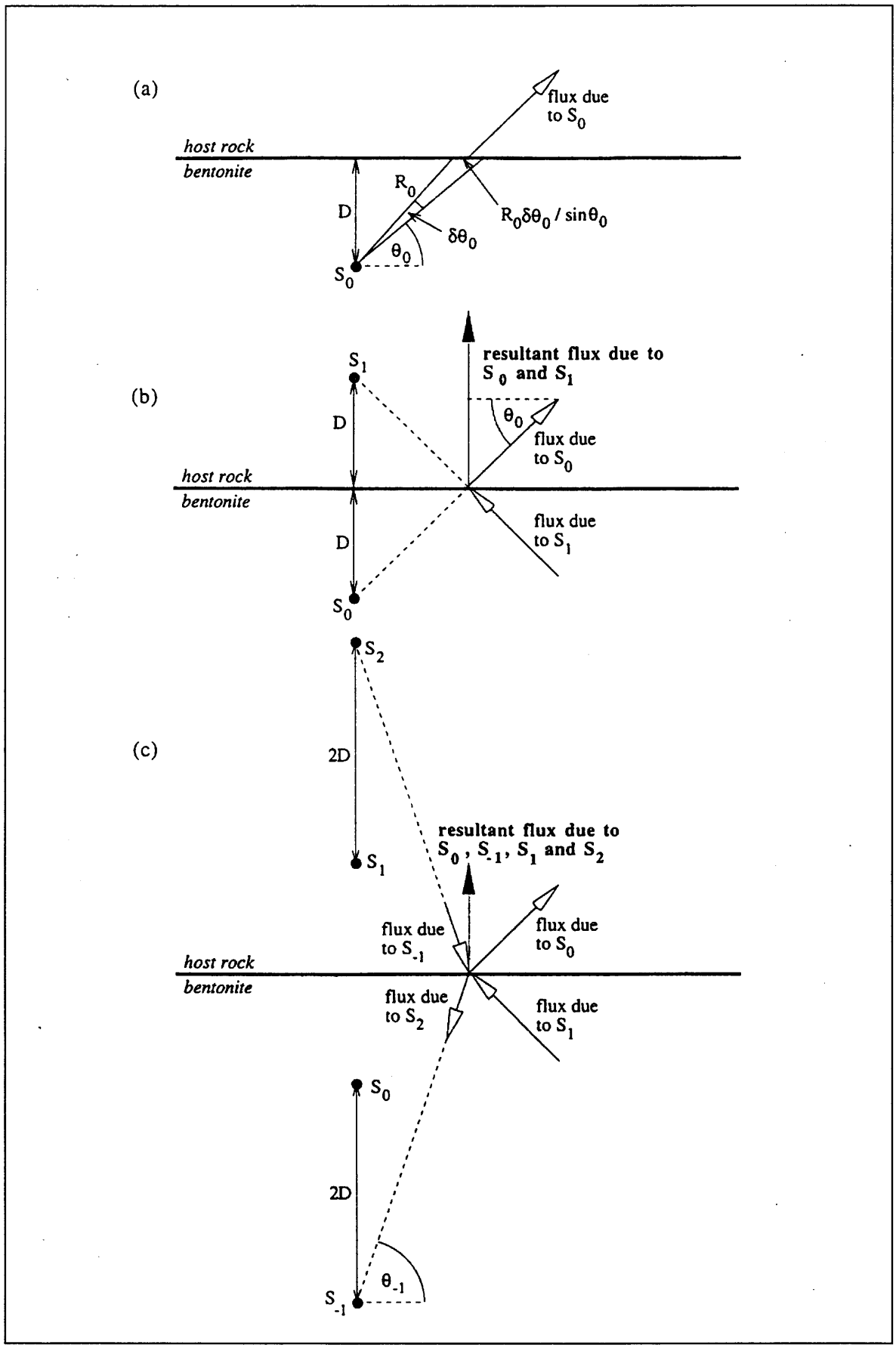

Figure III.3: Evaluation of flux across the bentonite-host rock interface.

The component parallel to the interface is cancelled by that due to the (oppositely signed) source S_1 (Figure III.3 (b)). The component of flux normal to the interface contributed by S_1 is, however, equal to that due to S_0: the combined flux due to the two sources is:

$$f_{b,0}+f_{b,1}=-\varepsilon_p D_p\left(\left.\frac{dC_{S_0}}{dr}\right|_{r=R_0}\sin\theta_0+\left.\frac{dC_{S_1}}{dr}\right|_{r=R_1}\sin\theta_1\right)=-2\varepsilon_p D_p\left.\frac{dC_{S_0}}{dr}\right|_{r=R_0}\sin\theta_0, \qquad \text{(III.15)}$$

since $C_{S_1}=-C_{S_0}$, $\sin\theta_1=-\sin\theta_0$ and $R_1=R_0$. The rate at which radionuclides from the two sources pass through the element is given by the product of the flux and the area of the element:

$$\left(f_{b,0}+f_{b,1}\right)\delta A=-4\pi r_b D\varepsilon_p D_p\frac{\delta\theta_0}{\sin^2\theta_0}\left.\frac{dC_{S_0}}{dr}\right|_{r=R_0}\sin\theta_0. \qquad \text{(III.16)}$$

Similarly, the combined flux due to the sources S_{-1} and S_2 (Figure III.3 (c)) is given by:

$$f_{b,-1}+f_{b,2}=-\varepsilon_p D_p\left(\left.\frac{dC_{S_{-1}}}{dr}\right|_{r=R_{-1}}\sin\theta_{-1}+\left.\frac{dC_{S_2}}{dr}\right|_{r=R_2}\sin\theta_2\right)=2\varepsilon_p D_p\left.\frac{dC_{S_0}}{dr}\right|_{r=R_{-1}}\sin\theta_{-1}, \qquad \text{(III.17)}$$

since $C_{S_{-1}}=-C_{S_2}=-C_{S_0}$, $\sin\theta_2=-\sin\theta_{-1}$ and $R_2=R_{-1}$. The rate at which radionuclides from the two sources pass through the element is given by the product of the flux and the area of the element:

$$\left(f_{b,-1}+f_{b,2}\right)\delta A=4\pi r_b D\varepsilon_p D_p\frac{\delta\theta_0}{\sin^2\theta_0}\left.\frac{dC_{S_0}}{dr}\right|_{r=R_{-1}}\sin\theta_{-1}. \qquad \text{(III.18)}$$

Summing the contributions from all such pairs of sources, the rate at which radionuclides pass through the element is given by:

$$\delta A\sum_{j=-\infty}^{\infty}f_{b,j}=-4\pi r_b D\varepsilon_p D_p\frac{\delta\theta_0}{\sin^2\theta_0}\sum_{i=0}^{\infty}(-1)^i\left.\frac{dC_{S_0}}{dr}\right|_{r=R_{-i}}\sin\theta_{-i}, \qquad \text{(III.19)}$$

where:

$$R_{-i}=\frac{(2i+1)D}{\sin(\theta_{-i})} \qquad \text{(III.20)}$$

and:

$$\theta_{-i} = \arctan\left[(2i+1)\tan(\theta_0)\right]. \tag{III.21}$$

Summing the contribution from all elements in the range $0 < \theta < \pi/2$, noting that an equal contribution to flux is provided by elements in the range $\pi/2 < \theta < \pi$, taking the limit $\delta\theta_0 \rightarrow 0$, and summing the contributions of N_c canisters, the rate at which radionuclides pass through the bentonite-host rock interface is given by:

$$F_b = -8\pi r_b' D\varepsilon_p D_p N_c \int_{\theta_0=0}^{\pi/2} \frac{d\theta_0}{\sin^2\theta_0} \sum_{i=0}^{\infty} (-1)^i \left.\frac{dC_{S_0}}{dr'}\right|_{r'=R'_{-i}} \sin\theta_{-i}\,. \tag{III.22}$$

Substituting Equation (III.8) in Equation (III.22), and eliminating C_D using Equation (III.10):

$$F_b = \frac{8\pi r_b' D\varepsilon_p D_p N_c C_0 \int_{\theta_0=0}^{\pi/2} \sum_{i=0}^{\infty} (-1)^i K_1(R'_{-i}) \sin(\theta_i) \dfrac{d\theta_0}{\sin^2(\theta_0)}}{K_0(r'_D)\left[1 + \dfrac{2}{K_0(r'_D)} \sum_{i=1}^{\infty} (-1)^i K_0(2iD')\right]}. \tag{III.23}$$

The concentration at an arbitrary point P (x,y) (Figure III.2) within the bentonite is also obtained by summing the contributions from all sources:

$$\frac{C}{C_D} = \frac{1}{K_0(r'_D)} \sum_{i=-\infty}^{\infty} (-1)^i K_0(r'_i), \tag{III.24}$$

where

$$r_i = \sqrt{x^2 + (y + 2iD)^2}\,. \tag{III.25}$$

Eliminating C_D using Equation (III.10):

$$\frac{C}{C_0} = \frac{\sum_{i=-\infty}^{\infty} (-1)^i K_0(r'_i)}{K_0(r'_D)\left[1 + \dfrac{2}{K_0(r'_D)} \sum_{i=1}^{\infty} (-1)^i K_0(2iD')\right]}. \tag{III.26}$$

C_0 appears in Equations (III.12) and (III.23) for radionuclide release rates into and out of the bentonite annulus, and also in Equation (III.26) for the concentration within the annulus. This unknown is determined by ensuring that solutions for the flux are continuous across the boundary between the crack and the bentonite annulus. The flux from the crack to the bentonite is also given by a solution of the diffusion equation within the crack (see Appendix II, Equation (II.6)). Equating this flux to that in Equation (III.12), rearranging and noting that $r_a' = r_a / \mu$ and $r_a'' = r_a / \mu_c$:

$$\frac{C_0}{C_s} = \left\{ \cosh(L'') + \frac{\mu_c K_1(r_D') \sinh(L'')}{\mu K_0(r_D') \left[1 + \frac{2}{K_0(r_D')} \sum_{i=1}^{\infty} (-1)^i K_0(2iD') \right]} \right\}^{-1} . \qquad \text{(III.27)}$$

Appendix IV - Sensitivity Analysis and Code Verification for the Modelling of Radiolytic Oxidation Fronts

(i) Simplified Solution

The summations expressed in Equation (47) are well approximated by their first term (i=1) if the non-dimensional distance ($r' = r / \nu$) is larger than ~ 3 and the crack aperture is small compared to the thickness of the bentonite. These conditions are generally satisfied in the calculations on the spreading of radiolytic oxidants presented in chapter 5.2.6. Thus, the following simplified solution applies:

$$\frac{C}{C_0} \cong \frac{K_0(r')}{B\, K_0(r'_D)}, \tag{IV.1}$$

where, after Equation (III.10)

$$B \equiv \frac{C_0}{C_D} \cong 1. \tag{IV.2}$$

and C_0, the oxygen concentration where the bentonite contacts the circumferential, water-filled crack, is given by Equation (50). Substitution of Equations (50) and (IV.2) in Equation (IV.1) yields:

$$C = \frac{S}{2\pi\, r'_a W \varepsilon_p D_p} \frac{K_0(r')}{K_1(r'_D)}. \tag{IV.3}$$

Equation (IV.3) can be used to examine the sensitivity of the distribution of radiolytic oxidants in the bentonite to, for example, the oxidant production rate (S), or to the crack width (W).

(ii) Influence of the Oxidant Production Rate on the Position of the Oxidation Front

Consider two oxidant production rates, denoted by S_α and S_β. If a particular oxygen concentration is found at a radial distance r_α from the crack for a production rate $S = S_\alpha$ and at a radial distance r_β for a production rate S_β, then, from Equation (IV.3):

$$\frac{S_\beta}{S_\alpha} = \frac{K_0(r'_\alpha)}{K_0(r'_\beta)} \tag{IV.4}$$

For arguments of K_0 larger than ~20, the following approximation holds (see, for example, LEBEDEW 1973)

$$K_0(r') \cong \sqrt{\frac{\pi}{2r'}} \exp(-r'), \tag{IV.5}$$

which, applied to Equation (IV.4), yields:

$$\frac{S_\beta}{S_\alpha} \cong \sqrt{\frac{r_\beta}{r_\alpha}} \exp\left[\frac{(r_\beta - r_\alpha)}{\nu}\right], \tag{IV.6}$$

or

$$2\frac{r_\beta}{\nu} + \ln r_\beta = \ln\left[r_\alpha \left(\frac{S_\beta}{S_\alpha}\right)^2\right] + 2\frac{r_\alpha}{\nu}. \tag{IV.7}$$

Equation (IV.7) is transcendental and can be solved iteratively. Calculations carried out with this simplified equation yield results in agreement with the small displacements predicted by the full model (Figure 6), supporting the finding that the production rate of radiolytic oxidants has only a small effect on the penetration depth of the oxidation front in the bentonite.

(iii) Influence of the Crack Width on the Position of the Oxidation Front

When the crack width is varied from a value W_α to W_β and the same oxygen concentration is found at radial distances r_α and r_β then, using $W = \pi r_D$, we get from Equation (IV.3):

$$\frac{W_\alpha}{W_\beta} = \frac{K_0(r'_\alpha)}{K_0(r'_\beta)} \frac{K_1(W'_\beta/\pi)}{K_1(W'_\alpha/\pi)}. \tag{IV.8}$$

This equation is transcendental and must be solved numerically for r_β. Results are shown in Figure IV.1, where the radial position of the 10^{-12} M oxygen isopleth is shown as a function of crack width for two values of [Fe(II)] and with all other parameters as given in Table 6. The plot shows that the position of the oxidation front is insensitive to crack width for apertures of less than ~ 1 mm. At larger crack widths, the front tends to expand, but the effect is negligible compared to the thickness of the bentonite (1.38 m). The effect on cracks wider than 1 cm is not shown because a) such apertures are unrealistic and b) a basic assumption of our model breaks down, namely the requirement that the crack width must be small compared to the thickness of bentonite, so that it can be treated as a line source.

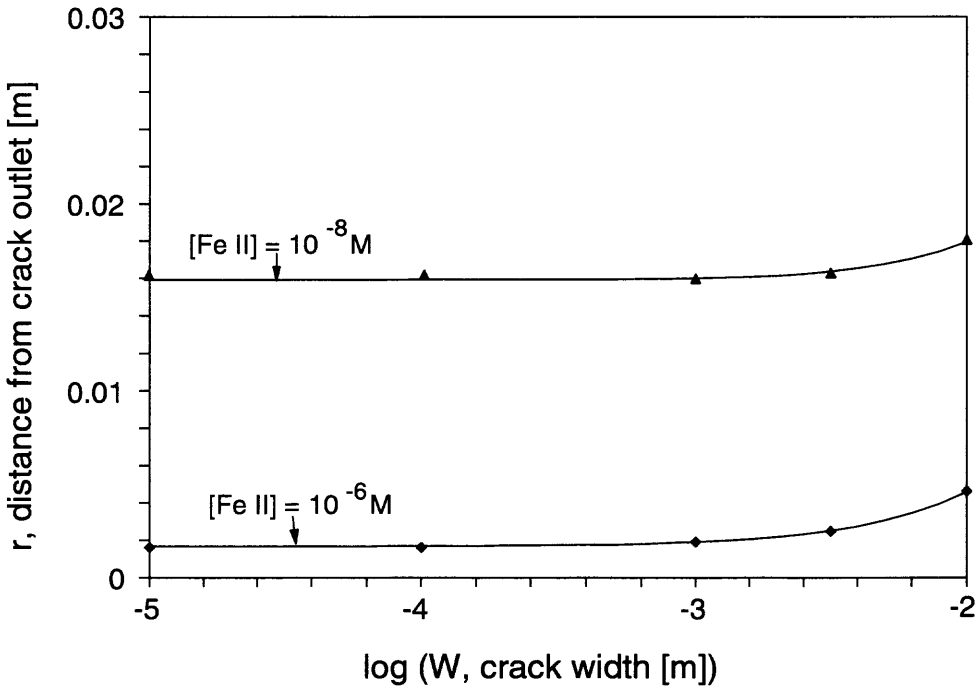

Figure IV.1: Sensitivity of the position of radiolytic oxidation fronts (defined as the 10^{-12} M oxygen-isopleth) to the aperture of the circumferential crack. The curves are obtained from the approximate solution given by Equation (IV.8), while symbols represent results obtained from the full solution given by Equation (47).

References

ABRAMOWITZ, M. & STEGUN, I. 1970: Handbook of Mathematical Functions (9th ed.); Dover Publications, New York.

AIDUN, C. K., BLOOM, S. G. & RAINES, G. E. 1988: Radionuclide Transport through Perforations in Nuclear Waste Containers; Mat. Res. Soc. Symp. Proc. Vol. 112, pp 261-272.

BATEMAN, K., ENTWISLE, D. C., KAMP, S. & SAVAGE, D. 1991: Bentonite-Groundwater Interactions: Results of Compression Rig Experiments; NAGRA Internal Report, NTB 91-53, NAGRA, Wettingen, Switzerland.

BÖRGESSON, L., HOEKMARK, H. & KARNLAND, O. 1988: Rheological Properties of Sodium Smectite Clay; SKB Technical Report 88-30, Stockholm, Sweden.

BURNS, W. G. et al. 1982a: Effects of Radiation on the Leach Rates of Vitrified Radioactive Waste; Journal of Nuclear Materials, vol. 107, pp 245-270.

BURNS, W. G. et al. 1982b: Effects of Radiation on the Leach Rates of Vitrified Radioactive Waste; Nature, v. 295, pp 130-132.

CHAMBRÉ, P. L., LEE, W. W. -L., KIM, C. L. & PIGFORD, T. H. 1987: Transient and Steady-State Radionuclide Transport through Penetrations in Nuclear Waste Containers; Mat. Res. Soc. Symp. Proc. Vol. 84, pp 131-140.

CURTI, E. 1995: Results of near-field transport calculations for the Kristallin-I safety assessment; NAGRA Internal Report, NIB 95-51.

EARY L.E. & SCHRAMKE J.A. 1990: Rates of inorganic oxidation reactions involving dissolved oxygen, in: Chemical modeling of aqueous systems II, D.C. Melchior and R.L. Bassett, eds., American Chemical Society, Washington, pp 379-396.

GODON, N. 1988: Effet des matériaux d'environnement sur l'altération du verre nucléaire R7T7 - Influence des argiles, Ph.D. thesis, Université d' Orléans, France.

GRINDROD, P., WILLIAMS, M., GROGAN, H. & IMPEY, M. 1990: "STRENG": a Source Term Model for Vitrified High Level Waste; NAGRA Technical Report Series, NTB 90-48, NAGRA, Wettingen, Switzerland.

IMSL, 1989: MATH/LIBRARY - FORTRAN Subroutines for Mathematical Applications, Edition 1.1, IMSL inc., Houston.

LEBEDEW, N. N. 1973: Spezielle Funktionen und ihre Anwendungen; Bibliographisches Institut, Wissenschaftsverlag, Mannheim, Germany, pp 371.

McKINLEY, I. G. 1985: The Geochemistry of the Near-Field; NAGRA Technical Report Series, NTB 84-48, NAGRA, Wettingen, Switzerland.

McKINLEY, I. G. & HADERMANN, J. 1985: Radionuclide Sorption Database for Swiss Safety Assessment; NAGRA Technical Report Series, NTB 84-40, NAGRA, Wettingen, Switzerland.

MEYER, R.J. & PETERS, F. 1927: Gmelins Handbuch der anorganischen Chemie, 8. Auflage: Wasserstoff, Deutsche Chemische Gesellschaft, Weinheim.

MITCHELL, J. K., SINGH, A. S. & CAMPANELLA, R. G. 1968: Soil Creep as a Rate Process; ASCE Journal of the Soil Mechanics and Foundations, 7 Divisions, Vol. 94, SM 1, pp 231-253.

NAGRA 1985: Project Gewähr 1985; Vols. 1-8, Vol. 9 (English Summary); NAGRA Gewähr Report Series NGB 85-01/09, NAGRA, Wettingen, Switzerland.

NAGRA 1994a: Conclusions from the Regional Investigation Programme for Siting a HLW Repository in the Crystalline Basement in Northern Switzerland; NAGRA Technical Report Series, NTB 93-09E, NAGRA, Wettingen, Switzerland.

NAGRA 1994b: Kristallin-I Safety Assessment Report; NAGRA Technical Report Series, NTB 93-22, NAGRA, Wettingen, Switzerland.

PEARSON F.J.,JR. & BERNER, U. 1991: Nagra Thermochemical Database - I. Core Data, NAGRA Technical Report Series, NTB 91-17, NAGRA, Wettingen, Switzerland.

PEARSON F.J.,JR. & SCHOLTIS, A. 1993: Chemistry of Reference Waters of the Crystalline Basement of Northern Switzerland for Safety Assessment Studies, NAGRA Technical Report Series, NTB 93-07, NAGRA, Wettingen, Switzerland.

RAI, D., FELMY, A.R. & RYAN, J.L. 1990: Uranium(IV) Hydrolysis Constants and Solubility Product of $UO_2.xH_2O$(am), Inorganic Chemistry, Vol. 29, pp 260-264.

RILEY, K. F. 1974: Mathematical Methods for the Physical Sciences; Cambridge University Press.

ROMERO, L., MORENO, L. & NERETNIEKS, I. 1995: Movement of a Redox Front around a Repository for High-Level Nuclear Waste; Nuclear Technology, Vol. 110, pp 238-249.

SNELLMAN, M., UOTILA, H. & RANTANEN, J. 1987: Laboratory and Modelling Studies of Sodium Bentonite Groundwater Interaction. In: Scientific Basis for Nuclear Waste Management X, Mat. Res. Soc. Symp. Proc. Vol. 84, pp 781-790.

STUMM, W. & MORGAN, J. J. 1981: Aquatic Chemistry; 2nd Edition, John Wiley & Sons, pp 780.

STUMM, W. & SULZBERGER, B. 1992: The Cycling of Iron in Natural Environments: Considerations based on Laboratory Studies of Heterogeneous Redox Processes; Geochim. Cosmochim. Acta, Vol. 56, pp 3233-3257.

SWALLOW, A. J. 1973: Radiation Chemistry, Longman, pp 275.

THURY, M., GAUTSCHI, A., MÜLLER, W. H., NAEF, H., PEARSON, F. J., VOBORNY, O., VOMVORIS, S. & WILSON, W. 1994: Geologie und Hydrogeologie des Kristallins der Nordschweiz; NAGRA Technical Report Series, NTB 93-01. NAGRA, Wettingen, Switzerland.

WANNER, H. 1985: Modelling Radionuclide Speciation and Solubility Limits in the Near-Field of a Deep Repository. In: Scientific Basis for Nuclear Waste Management IX, Mat. Res. Soc. Symp. Proc. Vol. 50, pp 509-516.

WHITTLE, A. J. & ARISTORENAS, G. 1991: Settlement of canisters in compacted bentonite; NAGRA Unpublished Report, NAGRA, Wettingen, Switzerland.

YAMAMOTO, Y. S. et al. (eds.) 1985: Ullmann's Encyclopaedia of Industrial Chemistry; Vol. A13, Weinheim, Germany, pp 446-461.

Acknowledgements

We would like to thank all our colleagues who took an interest in this work. Peter Jackson at AEA Technology and Bernd Grambow at Forschungszentrum Karlsruhe are gratefully acknowledged for their careful and constructive reviewing work. Special thanks are due to Urs Berner, Jörg Hadermann and Valérie Pot at PSI, and Jean-Claude Alder, Ingeborg Hagenlocher, Charles McCombie, Ian McKinley, Jürg Schneider and Piet Zuidema at NAGRA for fruitful discussions and helpful suggestions. Partial financial support by NAGRA is gratefully acknowledged.